

Geomorphometric descriptions of archipelagic aprons off the southern flanks of French Frigate Shoals and Necker Island edifices, Northwest Hawaiian Ridge

James V. Gardner[†], Brian R. Calder[†], and Andrew A. Armstrong[†]

Center for Coastal and Ocean Mapping–Joint Hydrographic Center, 24 Colovos Road, University of New Hampshire, Durham, New Hampshire 03824, USA

ABSTRACT

This study describes the geomorphometries of archipelagic aprons on the southern flanks of the French Frigate Shoals and Necker Island edifices on the central Northwest Hawaiian Ridge that are hotspot volcanoes that have been dormant for 10–11 m.y. The archipelagic aprons are related to erosional headwall scarps and gullies on landslide surfaces but also include downslope gravitational features that include slides, debris avalanches, bedform fields, and outrunners. Some outrunners are located 85 km out onto the deep seafloor in water depths of 4900 m. The bedforms are interpreted to be the result of slow downslope sediment creep rather than products of turbidity currents. The archipelagic aprons appear to differ in origin from those off the Hawaiian Islands. The landslides off the Hawaiian Islands occurred because of oversteepening and loading during the constructive phase of the islands whereas the landslides off the French Frigate Shoals and Necker Island edifices may have resulted from vertical tectonics due to the uplift and relaxation of a peripheral bulge or isolated earthquakes long after the edifices passed beyond the hotspot. The lack of pelagic drape in water depths above the 4600 m depth of the local carbonate compensation depth suggests that the archipelagic apron off the French Frigate Shoals edifice is much younger, perhaps Quaternary in age, than that off the Necker Island edifice, which has a 50 m pelagic drape. The pelagic drape off the Necker Island edifice suggests that the landslides may be as old as 9 Ma. The lack of pelagic drape off the French Frigate Shoals edifice suggests that the most recent

landslides are more recent, perhaps even Quaternary in age. The presence of a chute-like feature on the mid-flank of the French Frigate Shoals edifice appears to be the result of rejuvenated volcanism that occurred long after the initial volcanism ceased to build the edifice.

INTRODUCTION

Archipelagic aprons are submarine landslide complexes composed of erosion and depositional gravity flows that involve both sediment and blocks of the insular flanks. Aprons have been recognized as common bathymetric features on the lower flanks of oceanic islands, seamounts, guyots, and ridges for more than half a century. Archipelagic aprons have been extensively investigated with seismic reflection and single beam bathymetric profiling systems, especially in, but not restricted to, the Pacific Ocean (e.g., Hess, 1946; Kuenen, 1950; Dietz and Menard, 1953; Dietz et al., 1954; Hamilton, 1956; Menard, 1956, 1964; Shepard, 1963; Jones, 1967; Watts, 1978; Moore et al., 1989; Wolfe et al., 1994; Schmincke et al., 1995; Geisslinger et al., 1996; Funck et al., 1996; Goldstrand, 1998; Allen et al., 2007; Watt et al., 2012a, to cite a few studies). Interestingly, there are few documented historical submarine landslides composed entirely of submarine deposits (Watt et al., 2014). Since the advent of multichannel seismic reflection profiling and ocean drilling in the 1970s, studies stressed the significance of submarine erosion and gravity-driven downslope processes at the base of islands, seamounts, guyots, and ridges. Studies in the 1980s of landslides at seamounts, guyots, and islands used either long-range sidescan sonar (e.g., Moore et al., 1989; Masson et al., 1992) or utilized early versions of multibeam echosounders (MBES) but created only sidescan backscatter images (i.e., Moore et al., 1989; Holcomb and Searle, 1991), bathymetric contour maps (e.g., Hollister et al., 1978;

Vogt and Smoot, 1984; Smoot, 1985), or mesh grids (e.g., Taylor et al., 1975, 1980; Smoot, 1982, 1983a, 1983b, 1985). Recently, studies have utilized modern multibeam data (e.g., Deplus et al., 2001; Masson et al., 2002; Mitchell et al., 2002; Bohannon and Gardner, 2004; Silver et al., 2009; Casalbore et al., 2010; Montanaro and Beget, 2011; Watt et al., 2012b, 2014; Saint-Ange et al., 2013; Ramalho et al., 2015; Watson et al., 2017; Clare et al., 2018; Counts et al., 2018; Pope et al., 2018; Quartau et al., 2018; Santos et al., 2019; Casalbore et al., 2020) to provide complete, high-resolution digital terrain models of the geomorphology of various archipelagic aprons and submarine landslides. Although archipelagic aprons have never been described from this volcanically dormant area of the Northwest Hawaiian Ridge (Fig. 1), this study shows that this area is the site of numerous large archipelagic aprons.

During early stages of the formation of volcanic edifices, dike injection of pyroclastics and lavas rapidly loads and over-steepens the edifice flanks and creates instabilities that can lead to failures (McGuire, 1996, 2006; Mitchell, 2003). Once submerged, submarine weathering can begin to break down the volcanic flows that form the summit and upper flanks of these edifices. As weathering progresses, the volcanic rocks become weakened and gravity and seismic activity can exert enough force to eventually cause mechanical failure that breaks down the lava flows into smaller rocks and grain sizes (e.g., Jones, 1967; Keating and McGuire, 2000). Failure leads to slumps, landslides, turbidity flows, etc., that are composed of volcanoclastic debris that creates gravity-driven downslope processes that themselves further erode the flanks of islands, seamounts, and guyots and deposit material at the base of the edifices.

A depression of the underlying lithosphere and mantle is typically created beneath a large volcanic island (Fig. 2) as the active volcano grows in volume until the increased weight depresses the elastic lithosphere in the immediate

James Gardner  <http://orcid.org/0000-0002-6661-8204>

[†]Corresponding author: jim.gardner@unh.edu; brc@com.unh.edu; andy.armstrong@noaa.gov.

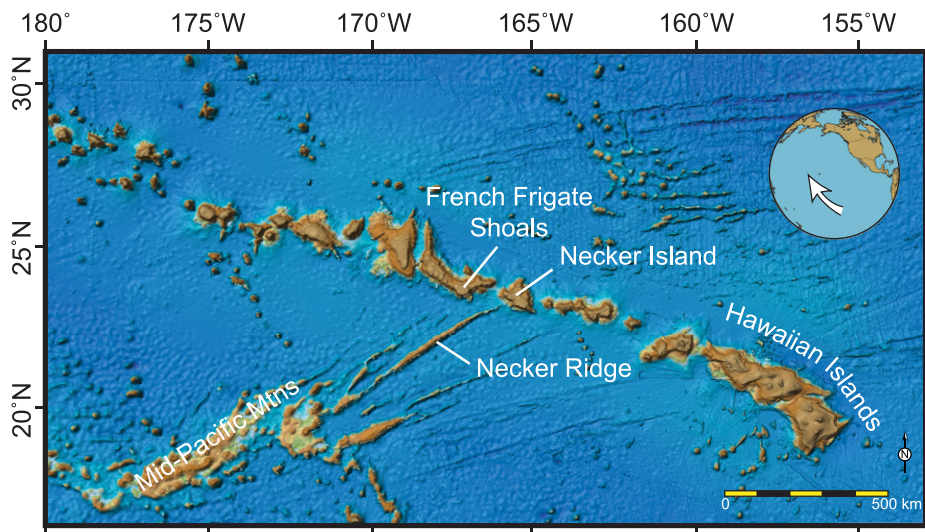


Figure 1. Map shows Global Multi-Resolution Topography bathymetry of the Hawaiian Ridge (from Ryan et al., 2009). Inset globe shows location of Hawaiian Ridge.

vicinity (e.g., Watts, 1978; Wolfe et al., 1994). The depressed lithosphere creates a moat that surrounds the island, seamount, or guyot that then becomes a depocenter for the downslope transported volcanoclastic material. The accumulations of the products of gravity-driven downslope processes at the base of individual islands, seamounts, and guyots were initially called “alluvial aprons” by Dietz and Menard (1953) and Dietz et al. (1954) and were formally defined as “archipelagic aprons” by Menard (1956). Menard (1956) also used the more general term “apron” where the archipelagic aprons of more than one seamount coalesced similar to a subaerial bajada (Fig. 3). Since the early investigations in the 1950s, many studies of archipelagic aprons have been published, and the explanation for the basic composition and construction of archipelagic aprons has remained little changed over the years. Although

Menard focused on the large regions of smooth morphology that surround groups of existing or drowned former islands, he incorrectly deduced that the majority of the aprons are composed of lava flows. Key discoveries since Menard’s studies conclude that (1) seamounts repeatedly build and collapse so that a greater volume of mass-wasted volcanoclastic material can accumulate as compared to the volume of a single complete seamount (e.g., Hunt and Jarvis, 2020); (2) the process of slope failure begins early in the history of a seamount, such that landslide debris is also a component of the internal structure of the seamount itself (e.g., Keating and McGuire, 2004); and (3) archipelagic aprons form around guyots and seamounts that have never been near or above sea level (e.g., Schmincke et al., 1995; Fig. 2). Large-scale, multiple collapses of island volcanoes are common features at several oceanic volcanic chains (e.g., Hawaiian Islands,

Moore et al., 1989; Marquesas Islands, Wolfe et al., 1994) that deliver volumes of poorly sorted volcanoclastic debris with a large range of sizes to the base of the island edifices and beyond.

Wolfe et al. (1994) carried out an extensive investigation of an archipelagic apron in the Marquesas Islands in the Pacific Ocean. Their study shows that the depression of the lithosphere is not always expressed in the bathymetry because the surrounding moat can be filled by a large volume of downslope-transported sediment. Eventually an archipelagic apron develops to the stage that the lower flanks of an edifice are buried, and the distal end of the archipelagic apron is interfingering with the basin sediments (Fig. 2). Wolfe et al. (1994, p. 13,592) comment that, “Catastrophic mass wasting occurred at several islands following construction...resulting in the disappearance of up to half of the subaerial structure...” Wolfe et al. (1994) comment that the mass-wasting material in their studies forms most of the archipelagic apron. In a similar study, Funck et al. (1996) found that the archipelagic apron of the Canary Islands in the Atlantic Ocean extends 44–74 km seaward of the edifice (Fig. 3). However, archipelagic aprons can extend out into the basin for hundreds of kilometers (Schmincke et al., 1995). The Gran Canaria archipelagic apron was drilled on Ocean Drilling Project Leg 157, and that drilling recovered interbedded volcanoclastic turbidites and extensive large-scale submarine slumps (Goldstrand, 1998). Gran Canaria is one of a series of closely spaced oceanic islands whose archipelagic aprons have coalesced into a submarine bajada (Fig. 3; note that the submarine bajada stands well above the depth of the older oceanic crust).

One of the distinguishing characteristics of archipelagic aprons is that they contain a chaotic assemblage of displaced blocks, debris avalanches, slumps, debris flow deposits, coarse- to fine-grained turbidites, and erosional channels and bedforms (e.g., Saint-Ange et al., 2013; Manville et al., 2009; Watt et al., 2014; Watt, 2015; Quartau et al., 2018). This assemblage produces a rough, blocky, textured seafloor, although turbidites produce a smooth seafloor, all of which can be easily mapped with modern multibeam echosounders. The rough-smooth boundary is clearly located as the change in MBES acoustic backscatter, where chaotic assemblages with rough and blocky surfaces generate acoustically high-backscatter that grades into a low-backscatter, fine-grained, smooth surface of pelagic sediments of the basin (Fig. 4). The massive submarine landslides off the Hawaiian Islands described by Lipman et al. (1988) and Moore et al. (1989) are an extreme class of archipelagic aprons (Fig. 5).

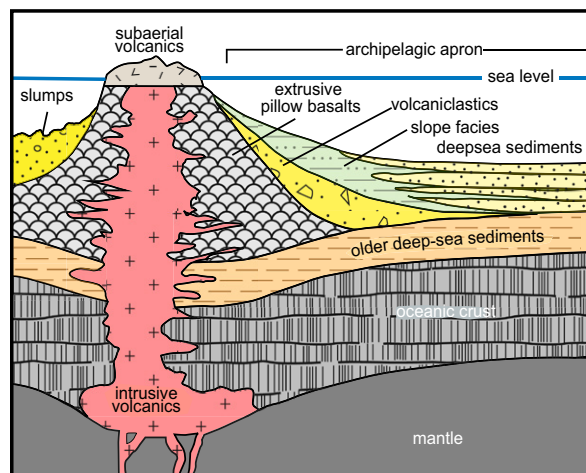


Figure 2. Internal architecture of a volcanic island is shown. Modified from Schmincke et al., (1995).

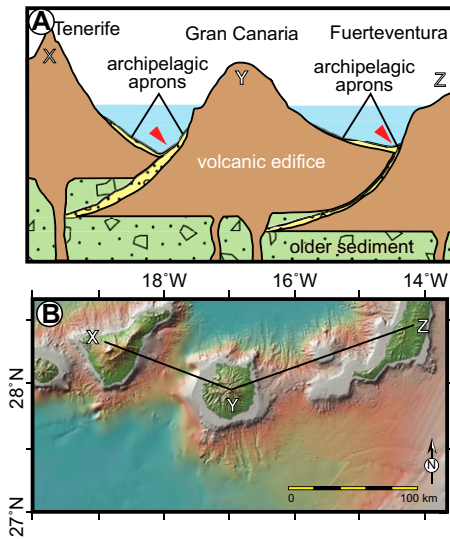


Figure 3. (A) Cross-section across three of the Canary Islands shows the interfingering (red arrows) of their individual archipelagic aprons (modified from Funck et al., 1996). (B) Map view of profile X-Y-Z. (C) Typical bajada from the California, USA, desert; white dashed lines indicate two alluvial fans that have coalesced into a bajada.

The landslides of the Hawaiian Islands were generated by the collapse of the volcanic islands while they were subaerial and under construction. The major flank collapses around the principal Hawaiian Islands generated enormous outrunner blocks that are found up to 140 km beyond the islands with vast areas of chaotic, hilly terrane that extend another 40 km beyond the outrunner blocks. The sizes of the displaced blocks found at the base of smaller islands, sea-

mounts, and guyots are generally much smaller and have shorter runout distances (e.g., Moore and Clague, 2002) than the massive Hawaiian Islands examples. However, there have yet to be any studies as to whether individual Hawaiian Islands landslides are the result of a single extreme-magnitude event or the products of longer-term accumulations of multiple smaller events, as Masson et al. (2002) have demonstrated in the western Canary Islands.

The present study uses complete, latest-generation multibeam coverage (Fig. 6) and more than 5000 line km of co-collected sub-bottom profiler data to quantitatively describe the surface expressions of the various components that make up the archipelagic aprons on the south side of the French Frigate Shoals and Necker Island edifices.

DATA SOURCES AND METHODS

The data used in this study were acquired on three cruises dedicated to MBES mapping of Necker Ridge, a volcanic ridge that strikes to the SW almost perpendicular to the Northwest Hawaiian Ridge at the Necker Island edifice (Gardner et al., 2013). The first cruise used the National Oceanic and Atmospheric Administration (NOAA) Ship *Okeanos Explorer* (EX0909L1) equipped with a 30 kHz Kongsberg Maritime EM302 MBES (Malik et al., 2009) and the other two cruises (KM1121 and KM 1718) were on the RV *Kilo Moana* equipped with a 12-kHz Kongsberg Maritime EM122 MBES (Gardner and Calder, 2011; Armstrong and Calder, 2017). The senior author processed all of the data post-cruise for this study using QPS/Fledermaus and QPS/Qimera to process and analyze the bathymetry. QPS/FMGT was used to process the acoustic backscatter. The MBES

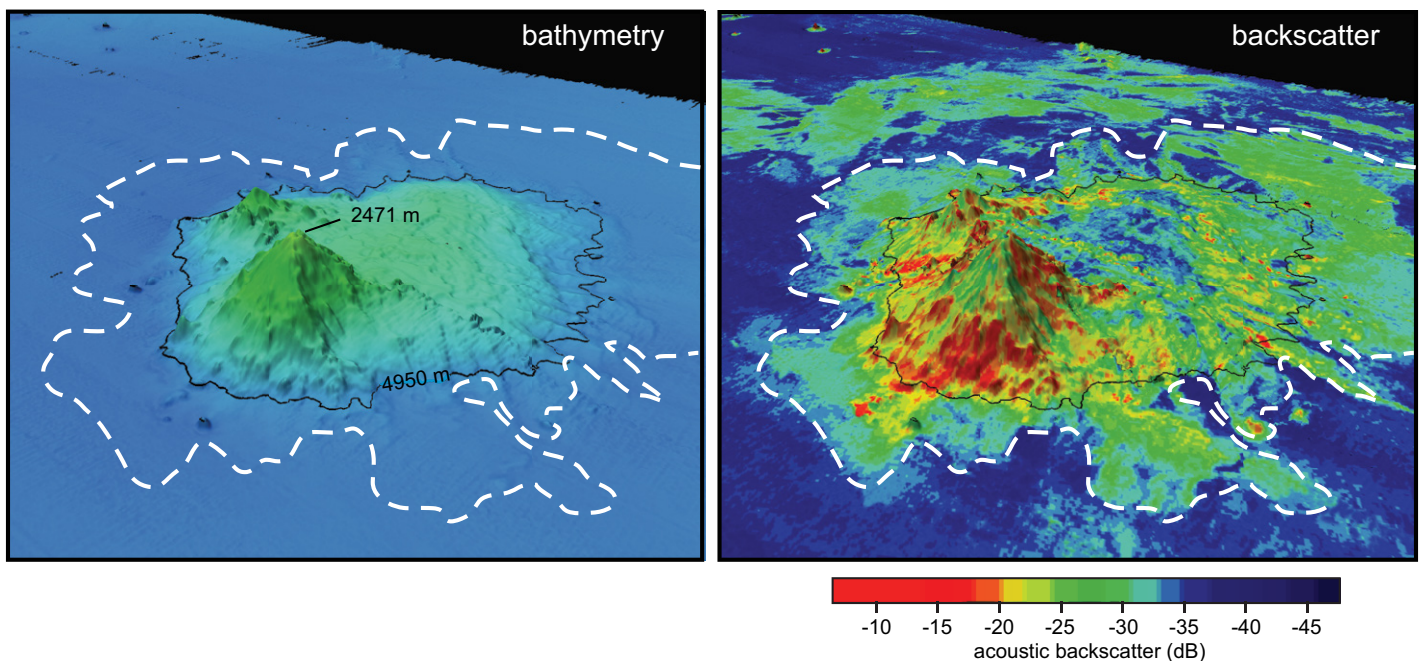


Figure 4. Perspective views are shown of bathymetry (left) and multibeam acoustic backscatter (right) of a central Pacific seamount with the 4950 m isobath (black line), which outlines the base of the volcanic edifice. The bathymetric relief of the archipelagic apron extends for 45 km (SW to NE), whereas the backscatter extends for 72 km along the same profile. The high backscatter (>−30 dB) that extends beyond the 4950 m isobath is caused by the roughness of the archipelagic apron as compared to the smoother, lower backscatter (<−35 dB) basin sediments. Data from Gardner (our data).

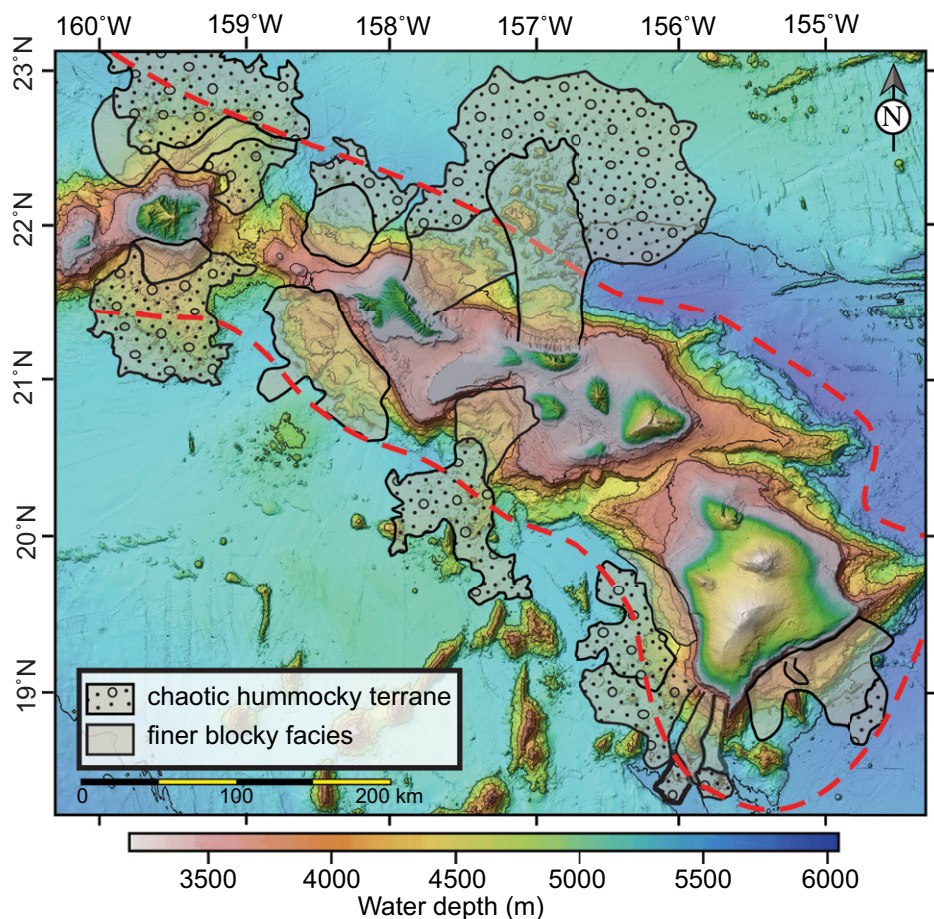


Figure 5. Map shows massive landslides of the Hawaiian Islands superimposed on Global Multi-Resolution Topography bathymetry. Dashed red line marks the axes of the Hawaiian Deep. Modified from Moore et al. (1989).

bathymetry and acoustic backscatter were gridded at 50 m/pixel. Background bathymetry from GeoMapApp/GMRT v. 3.6.10 (Ryan et al., 2009) was gridded at 225 m/pixel. In addition to the collection of MBES data, both RV *Kilo Moana* cruises collected continuous sub-bottom profiler (SBP) data with a Knudsen 3260 system with a manufacturer-specified vertical resolution of 1 m in water depths deeper than 1000 m. All of the data used in this paper are publicly available at the NOAA National Centers for Environmental Information (<https://maps.ngdc.noaa.gov/viewers/bathymetry/>).

TERMINOLOGY

The term “archipelagic apron” recently has been renamed “volcaniclastic apron,” but the original term is used here because of its historic usage in the large volume of marine geology literature on the subject. French Frigate Shoals is an atoll that developed on top of a large submerged, relatively flat volcanic ridge

with several submerged banks less than 60 m below sea level on the ridge summit. Necker Island is a small remnant of an island on a submerged shield volcano with a surface that is almost completely eroded to less than 50 m water depth. Archipelagic aprons are found at the southern bases of the two edifices. A rich and varied taxonomy for classifying landslides exists (e.g., see discussions of Hungr et al., 2001; Masson et al., 2002). The present work is based solely on MBES bathymetry and backscatter data and SBP profiles, and assumptions are made about the composition of the sediment based on acoustic backscatter. Assumptions of sediment facies were made because there are few sediment samples in the study area. Also, to apply most landslide classifications, the type of rock or sediment has to be known and assumptions have to be made as to whether the failures were sudden and the transport rapid or the failures were prolonged and the transport slow. For example, Hungr et al. (2001) define a rock avalanche as a failure of a rock slab that disintegrates and rapidly

moves as an unchannelized granular flow. They apply the term debris avalanche to a mixture of sediment and large clasts, but they do not define the lower limit of clast size. As for the material of a failure, Watt et al. (2012a, 2012b) use a terminology that describes a landslide as a generic term for a gravity-driven failure of rock or sediment without any implications for the processes that may characterize the movement. They use volcanoclastic for any sediment derived from a flank collapse of a volcanic edifice, and they use seafloor sediment for any pre-existing sediment that became incorporated in the final landslide deposit. A headwall is a large, arcuate-shaped embayment into the upper flank and platform of a volcanic edifice. A slide is defined here as a large, relatively coherent, intact feature with steep sides that resides immediately below a headwall scarp and rests on the scarp surface.

The distinctions between types of submarine landslides are difficult to make in the present study because of the lack of sample data, so the term debris avalanche is used for high-backscatter zones below gullies (e.g., Laberg and Vorren, 2000; Posamentier and Kolla, 2003; Gee et al., 2005) at their upper end followed by a mottled high- and medium-backscatter texture with numerous large blocks scattered throughout the deposit and ending in featureless, low-backscatter sediment. Undoubtedly, this assignment can include debris flows and even turbidites (see Watt et al., 2014). Gullies are clearly delineated in the acoustic backscatter images as MBES high-backscatter lineations (typically at least 20 dB higher backscatter than the intervening areas) that are braided and eventually converge down the fall line of a slope. Gullies are often subtle in the MBES bathymetry that suggests gully relief of only a meter or two. Bedforms were identified as a field of linear to arcuate crests and troughs that are generally concave downslope and perpendicular to the downslope gradient. Outrunner field is used for areas of medium backscatter that contain scattered and isolated large blocks with high backscatter. The area beyond the mottled medium backscatter texture is considered deep sea sediments because these areas have very low relief, very low gradients, and no resolved blocks.

THE AREA

French Frigate Shoals and Necker Island exist along the summit of the middle of the long-dormant Northwest Hawaiian Ridge (Fig. 1). The French Frigate Shoals atoll (also called Kānemiloa'i) sits on a relatively flat, oval-shaped surface at water depths less than 40 m deep. The oval-shaped surface rises above a crescent-shaped

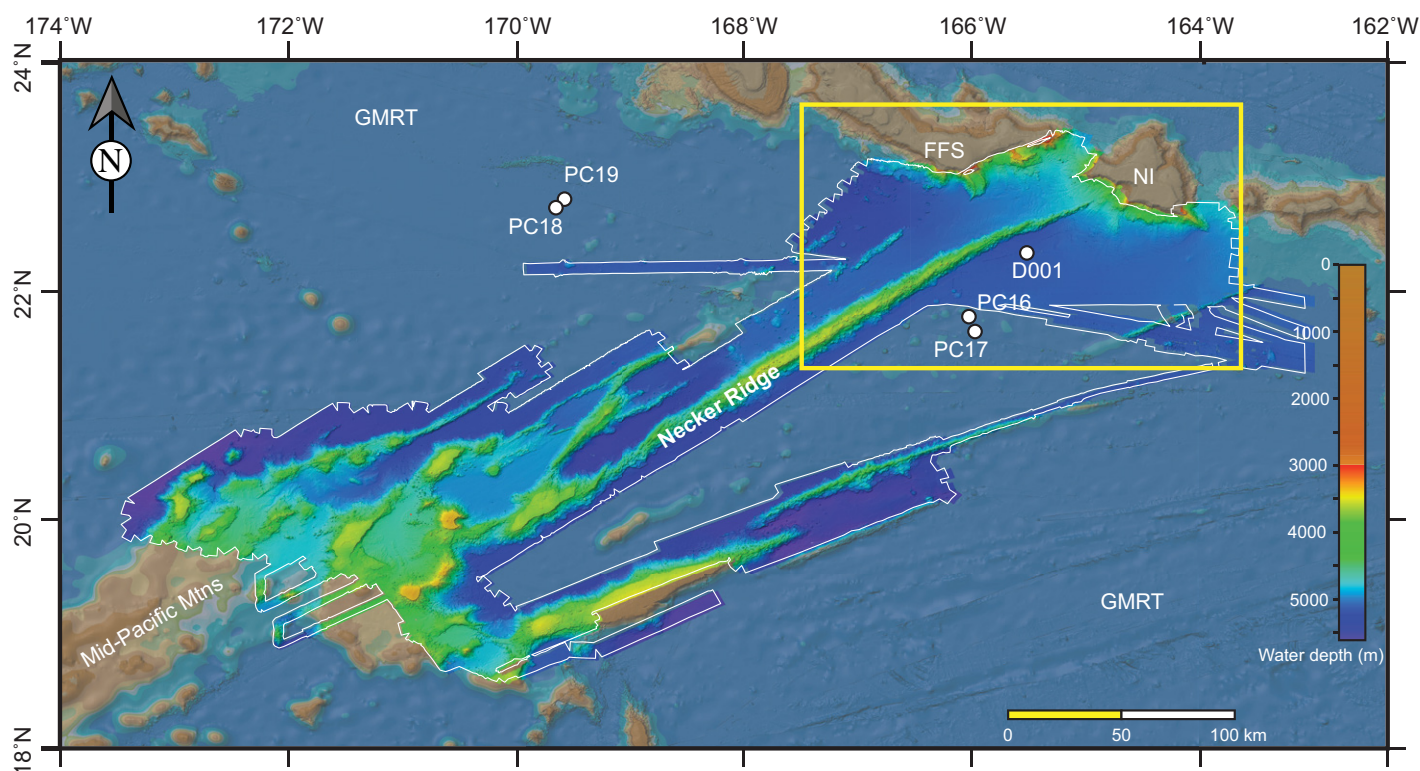


Figure 6. Overview map shows bathymetry of a section of the mid-Hawaiian Ridge and Mid-Pacific Mountains in the vicinity of the French Frigate Shoals (FFS) and Necker Island (NI) edifices. Yellow rectangle encloses the study area. White circles indicate locations of piston cores (PC) in area. Color scale applies only to multibeam echosounder (MBES) bathymetry. Global Multi-Resolution Topography (GMRT) bathymetry appears in the background (Ryan et al., 2009). Brighter colored areas indicate MBES bathymetry.

platform at water depths less than 800 m deep. The atoll is a remnant of a volcano that has been eroded and now stands only 37 m above sea level (Rooney et al., 2008). Necker Island (also called Mokumanamana) rises from a platform in water depths of less than 40 m that is a remnant of a much larger volcano with a peak that now stands 84 m above sea level (Rooney et al., 2008). Dalrymple et al. (1974) and Clague and Dalrymple (1989) provide the only reported K-Ar dates from Necker Island and French Frigate Shoals. Their data give weighted mean ages for French Frigate Shoals (two samples) of 11.7 Ma and Necker Island (two samples) of 10.3–10.0 Ma. These dates indicate that the erosion and eventual downslope transport of debris began sometime after these dates as evidenced by the surface expression of the debris (see below).

Necker Ridge is a submarine ridge composed of stacked volcanic lava flows, rather than volcanoclastic or pyroclastic deposits, that strikes almost 90° toward the Necker Island edifice (Gardner et al., 2013). The ridge spans the area between the southern flank of the Necker Island edifice on the northeast to the Mid-Pacific Mountains on the southwest (Figs. 1 and 6). The summit of the ridge plunges to the northeast as it approaches the Necker Island edifice and is

buried by an archipelagic apron. Rocks from Necker Ridge have been dated at 82.5 Ma (Saito and Ozima, 1977) and ca. 71 Ma (Clague and Dalrymple, 1975).

THE SOUTHERN FLANKS OF FRENCH FRIGATE SHOALS AND NECKER ISLAND EDIFICES

The French Frigate Shoals edifice is connected to the Necker Island edifice by a 45-km-wide, 3400-m-deep saddle that stands ~900 m above the flanking deep seafloor (Fig. 7). Two separate archipelagic aprons occur on the lower flanks of the French Frigate Shoals edifice, and there is a large archipelagic apron on the southwest-facing flank and a much smaller one on the southeast-facing flank (Fig. 7). Sediment derived from the southwestern flank of the Necker Island edifice was directed both north and south of the barrier of Necker Ridge (Fig. 7). The flanks of both edifices have slopes of 10° to 35° in water depths that increase from 500 m to 4000 m. The following sections discuss observations that show that the southern margins of the two edifices are dominated by: (1) head scarps on the uppermost flanks and summit edges of edifices, (2) gullies below the head scarps that represent the upper unit of

the archipelagic apron, followed by (3) fields of bedforms on the lower flanks of the archipelagic aprons and (4) debris avalanches that form the seaward limit of the archipelagic aprons. Within the debris avalanches, (5) fields of isolated outrunner blocks are scattered on the deep seafloor.

Southern Archipelagic Aprons of the French Frigate Shoals Edifice

The French Frigate Shoals edifice is composed of a relatively flat and featureless 900 km² platform that varies in water depths less than 40 m deep and is located at the southern edge of a 200-km-long middle section of the Northwest Hawaiian Ridge. This platform, and four smaller platforms at similar water depths, rise from a somewhat crescent-shaped and smooth ridge at 400–800 m water depth (Fig. 7). The southern edge of the deeper platform and the southern flank of the French Frigate Shoals platform have crescent-shaped headwall scarps eroded into their upper edges. The scarps range from 2 km to 12 km wide with scarp-face relief from 250 m to 1400 m high. The areas immediately below the headwall scarps have gradients of 10° to steeper than 25°. Where mapped by MBES, a

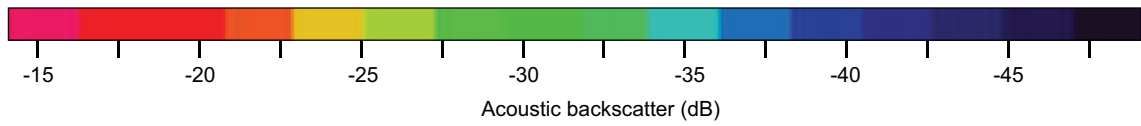
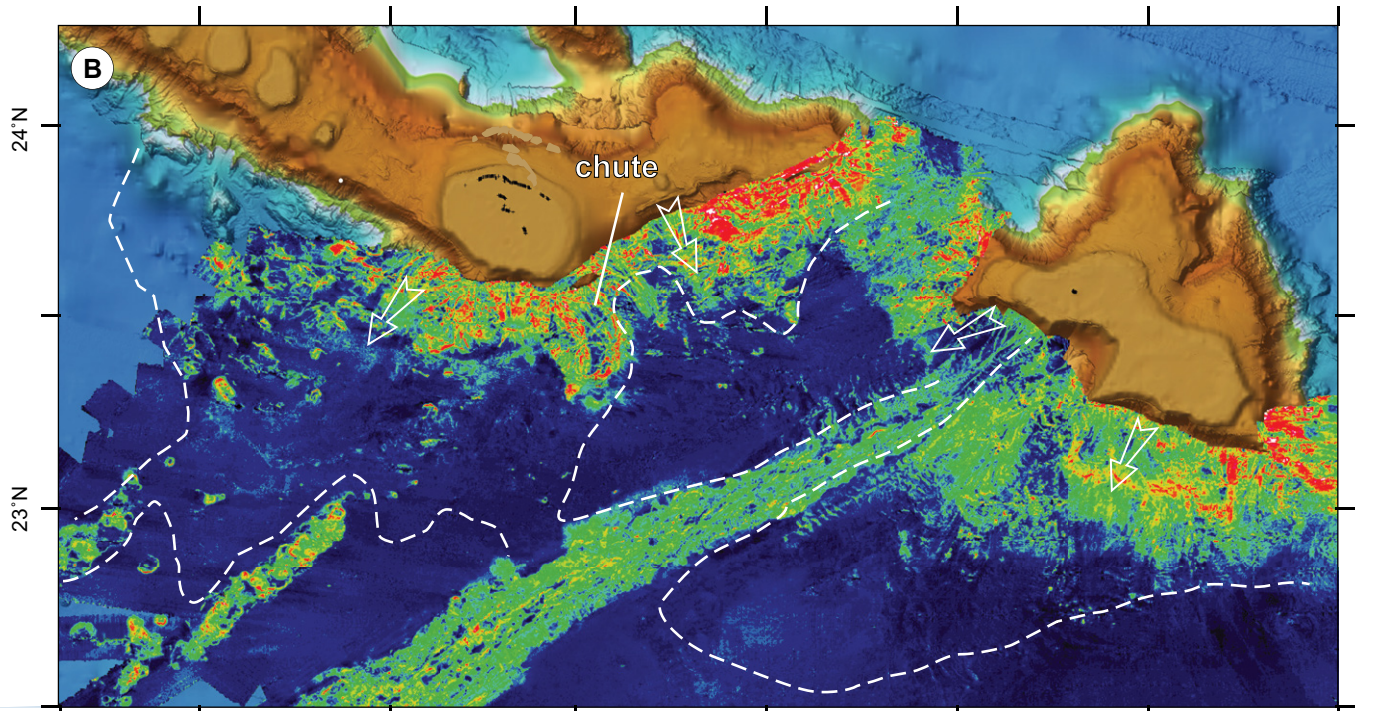
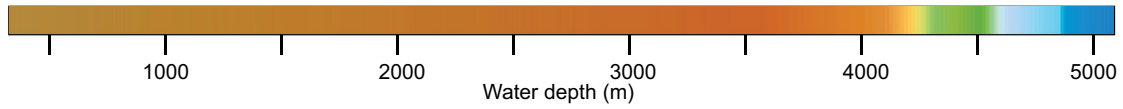
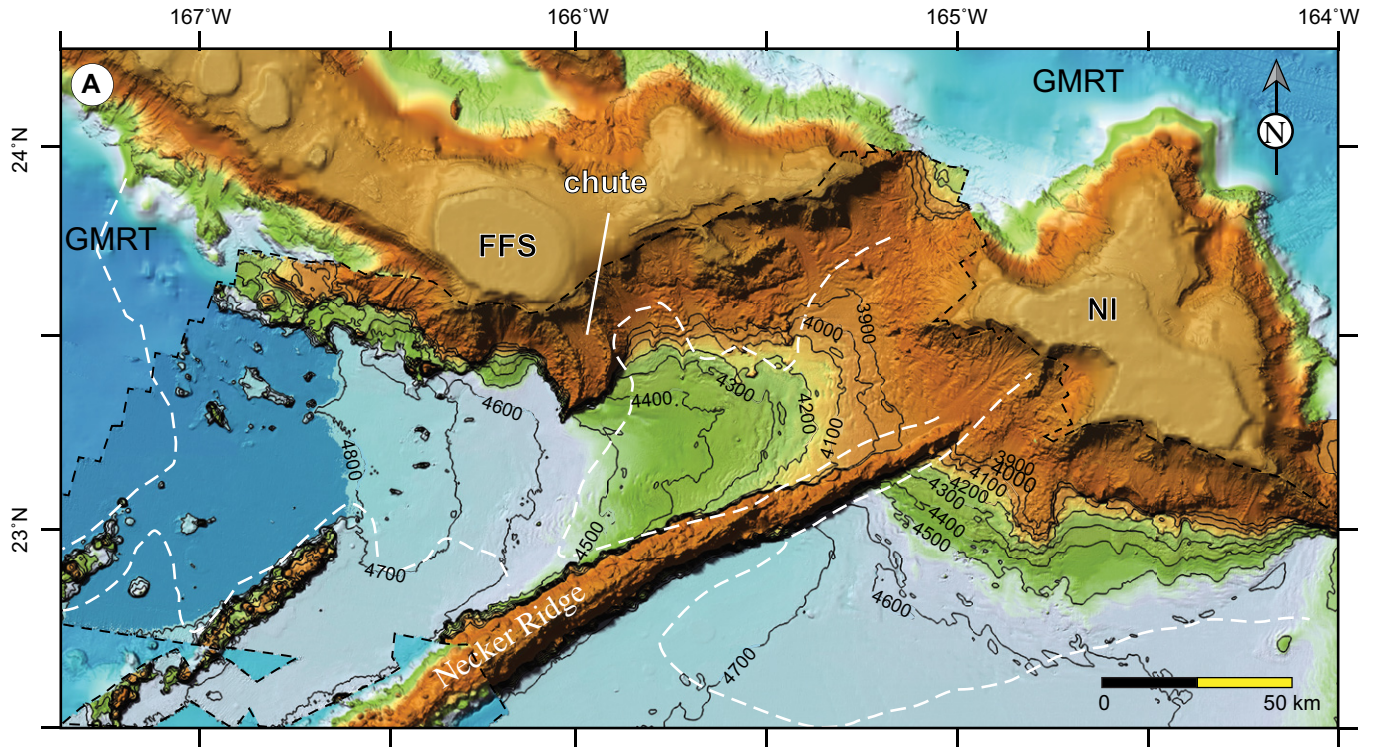


Figure 7. (A) Multibeam echosounder (MBES) bathymetry of southern archipelagic aprons of French Frigate Shoals (FFS) and Necker Island (NI) edifices with the extent outlines in black dashed lines. White dashed lines outline the extent of the archipelagic aprons; see text for discussion of chute. Selected isobaths in meters. **(B)** Same area as A, but of MBES acoustic backscatter. White arrows show transport directions. Color scale applies only to MBES backscatter. GMRT—Global Multi-Resolution Topography.

significant portion of the upper flanks directly below the headwall scarps have numerous linear downslope-trending, high-backscatter gullies (Figs. 8 and 9) that occur in water depths that range from less than 1300 m to 4150 m. The gullies have backscatter values of -22 dB to -18 dB, whereas the intervening areas have

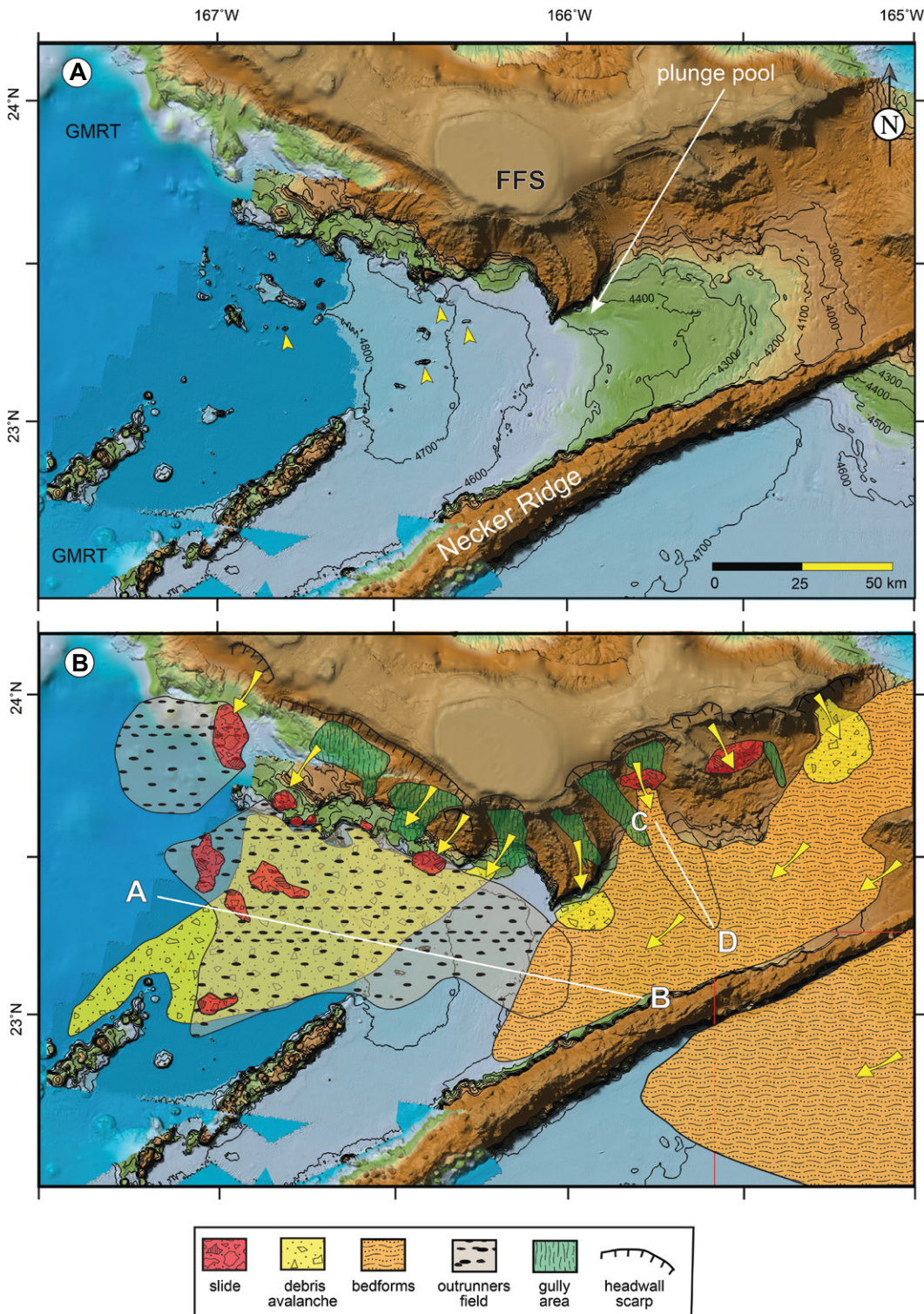


Figure 8. (A) Close-up view of multibeam echosounder (MBES) bathymetry of archipelagic apron off French Frigate Shoals edifice (FFS) with MBES extent outlined in Figure 7A. Yellow arrowheads point to outrunners profiled in Figure 11. See Figure 7A for bathymetry color scale. **(B)** Same view as in (A) with interpretations of components of the archipelagic aprons. Profile A–B is the sub-bottom profile in Figure 12 that shows the 3.5 kHz signatures of the various facies of the archipelagic apron. Bathymetric profile C–D is shown in Figure 15. **(C)** Same area as (A) of MBES acoustic backscatter of French Frigate Shoals archipelagic apron. **(D)** Interpretation of components of the archipelagic aprons outlined on the acoustic backscatter image.

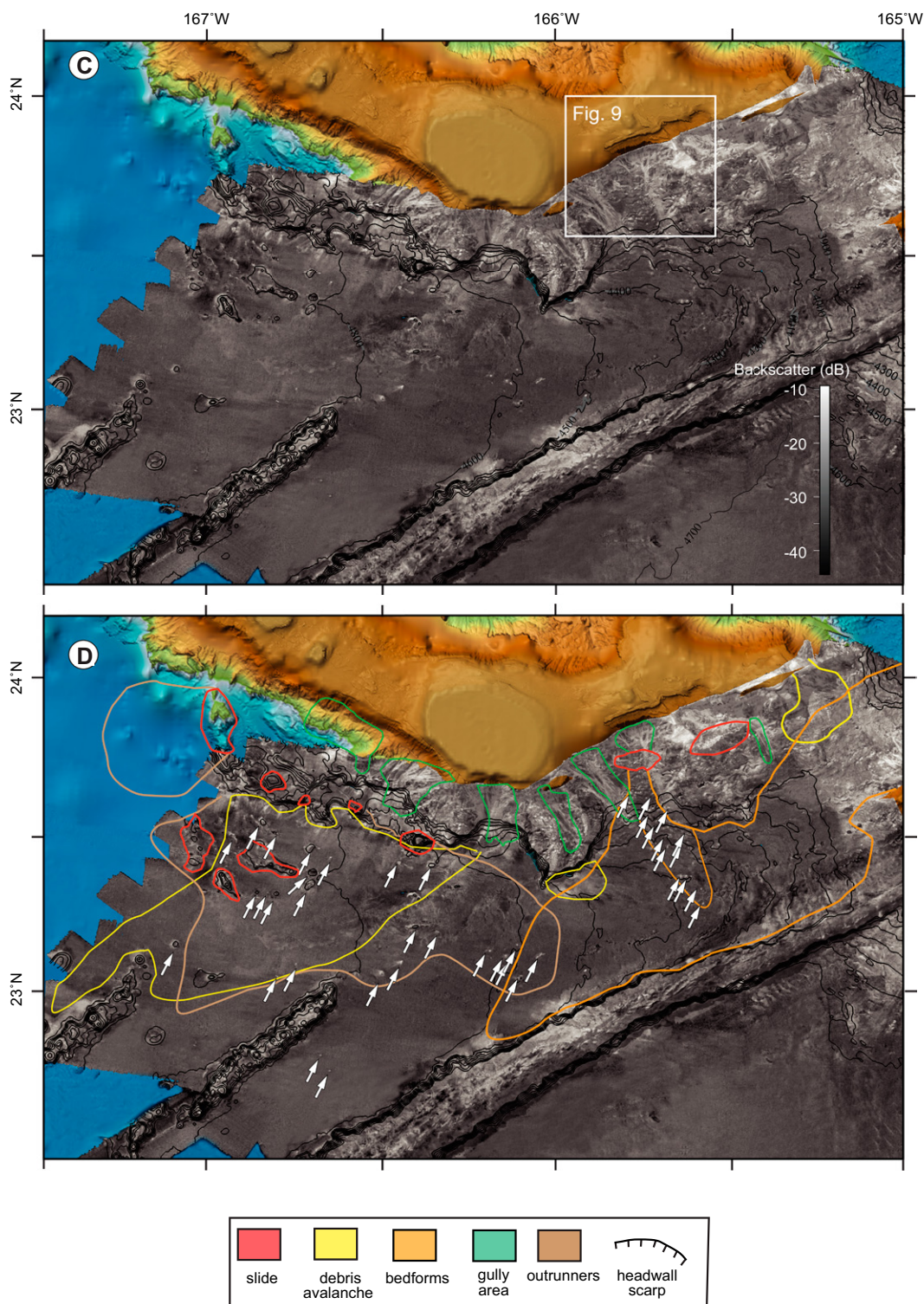


Figure 8. (Continued)

values of -38 dB to -35 dB. Some of the gullies have as much as 20 m of relief below the adjacent inter-gully areas (Fig. 9). The gullies vary in widths from 0.3 km to 1.6 km and extend downslope for 26 km. Many of the gullies cross one another, and there is a tendency for the gullies to converge downslope. The south-

ern flank of the edifice below the gullies descends to the deep seafloor with gradients that decrease from $\sim 10^\circ$ in the upper kilometer to less than 1° at the deep seafloor.

Slides occur within the area of gullies and are scattered from the upper and mid flank to the base of the edifice and as far out as 80 km onto

the deep seafloor (Fig. 8). Slides were arbitrarily differentiated from outrunners (see below) as large, high-backscatter (-38 dB to -21.5 dB) features with a high degree of surface relief. Although the basal dimensions of slides are easy to determine from the MBES bathymetry, the volume of each slide is almost impossible to

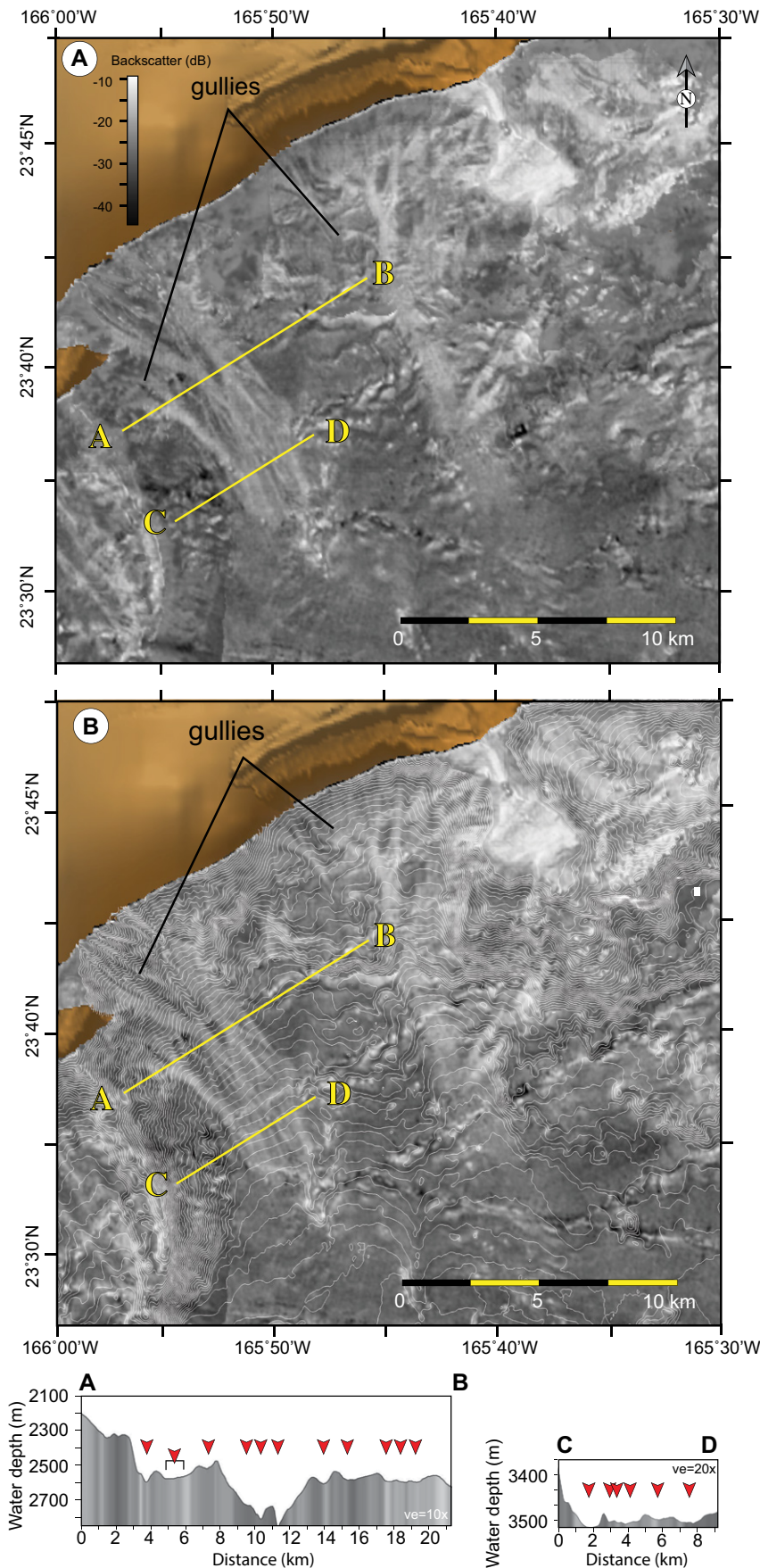


Figure 9. (A) Example shows multibeam echosounder, high-backscatter linear striations below headwall scarps on French Frigate Shoals. Brown area is Global Multi-Resolution Topography bathymetry (Ryan et al., 2009). (B) Same area with 50 m isobaths from 1200 m to 4300 m. Profiles A–B and C–D show gully relief (red arrowheads). See Figure 8C for location.

accurately determine because of their complex vertical relief. Nevertheless, an estimate of slide volume (V_s) was attempted with measurements of the maximum and minimum basal lengths (L_{max} and L_{min} , respectively) and one-third of the measured maximum height (H) and by applying the formula for a rectangular pyramid, where:

$$V_s = (L_{max} * L_{min}) * H / 3 \quad (1)$$

The slides range in estimated volume from 0.1 km^3 to 6.1 km^3 yet show no correlation of slide volume to seafloor gradient or distance from the base of the edifice (Figs. 10A–10B).

Outrunners occur as both single and aggregated, high-backscatter (–20 dB to –16 dB), isolated large blocks scattered on the otherwise low-backscatter (–39 dB to –38 dB) seafloor (Fig. 8B). Outrunners are found close to the base of the edifice as well as 85 km out onto the deep seafloor, where gradients are less than 1°. Outrunners are somewhat elongated in shape (Fig. 10C) and vary in height from 2 m to 95 m with distance from the edifice flank, and many have sediment banked on the upslope side and shallow moats with 3–15 m on the downslope sides (Fig. 11). There is no correlation of the presence of a sediment bank or moat with distance from the edifice flank. Estimates of outrunner volume (V_b) used the formula for a rectangular pyramid (Equation 1) as well as the formula for a right circular cone (Equation 2), where:

$$V_b = \pi R^2 H / 3 \quad (2)$$

with the radius (R) is half of the average of the measured basal long and short lengths and (H) is the tallest height of the outrunner. The results of outrunner volume calculated from Equation 1 and Equation 2 (Fig. 10F) shows that there is little difference from either equation in the estimated outrunner volumes. Outrunners with estimated volumes larger than $\sim 1.5 \text{ km}^3$ are found between 10 km and 50 km from the base of the edifice, whereas smaller outrunners ($< 0.5 \text{ km}^3$ in volume) are found scattered from $< 5 \text{ km}$ to 85 km from the base.

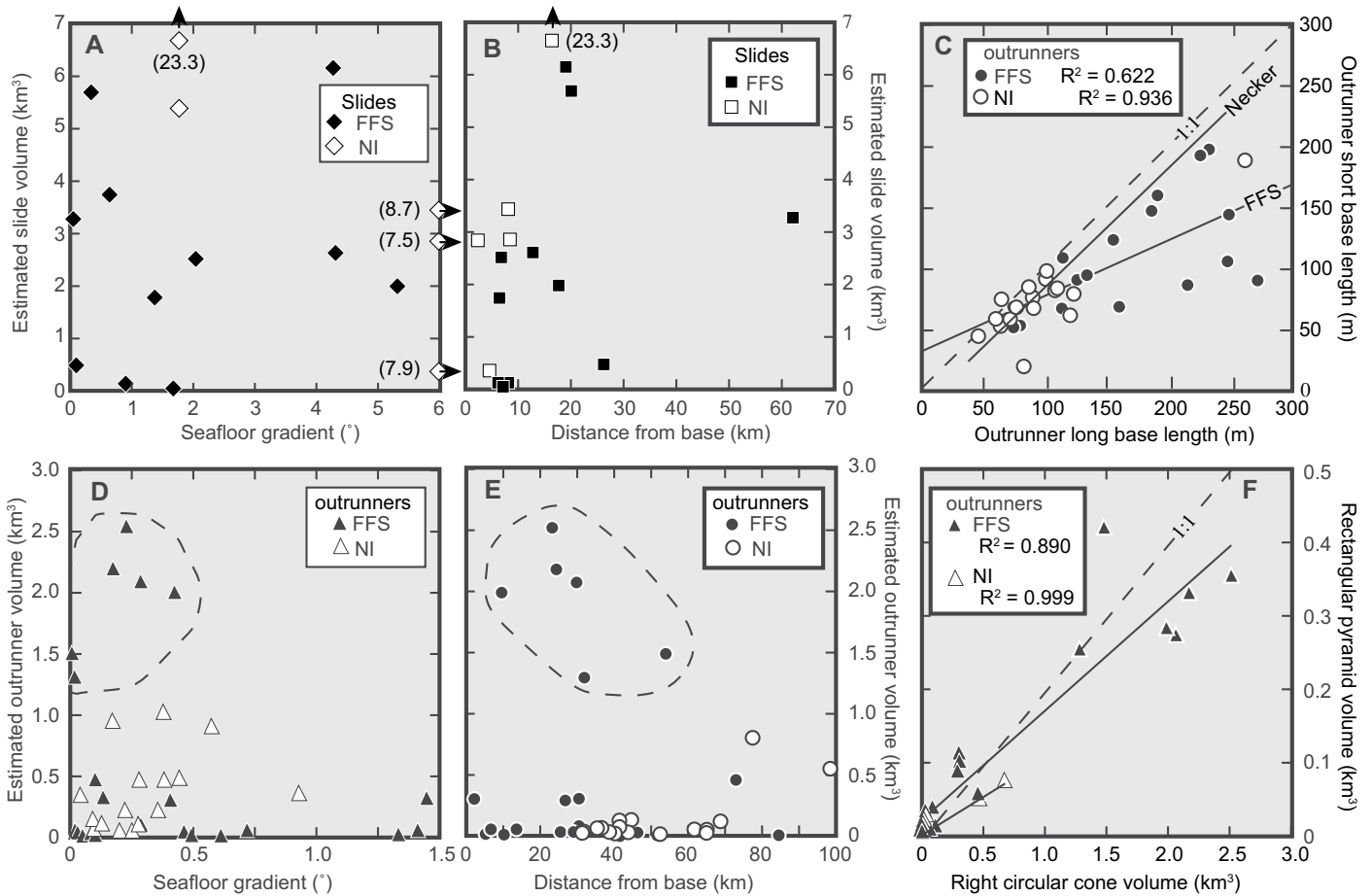


Figure 10. Plots of (A) French Frigate Shoals (FFS) and Necker Island (NI) edifices estimate slide volume vs. seafloor gradient and (B) distance from the base of the edifice. (C) Plot of long base length vs. short base length of outrunners off FFS and NI edifices. (D) Plots of estimated outrunner volumes (see text) vs. seafloor gradients. (E) Distance from the base of the edifices (dashed ellipses encircle anomalously large-volume outrunners). (F) Plot of right circular cone volume vs. rectangular pyramid volume for FFS and NI edifice outrunners.

Debris avalanche deposits are interpreted as areas generally deeper than 4000 m water depth that have backscatter values of -34.5 dB to -33 dB as compared to values of -39 dB to -38 dB of the deep seafloor (Fig. 8). They have a distinctive hummocky, strong surface reflection and show little or no 3.5 kHz penetration on SBP records (Fig. 12). Three debris avalanches were mapped in the French Frigate Shoals edifice archipelagic apron. The largest debris avalanche covers an area of 4250 km² and extends at least 100 km beyond the flank of the edifice. The other two debris avalanches are much smaller; they cover areas of 370 km² and 140 km². A plot of width versus length of the debris avalanches shows that the largest one is elongate to radial in surface aspect (Fig. 13), an aspect that correlates with a relatively cohesive runout flow with a major fine-grained component of the facies (Masson et al., 2002; Masson, 2006; Watt et al., 2014). The 370 km² debris avalanche has an aspect between elongate to radial, whereas

the smallest deposit is radial. Watt et al. (2014) suggest that these two aspect ratios indicate cohesive to cohesionless flows, respectively. The higher backscatter values and SBP acoustic response suggest that all of the debris avalanches are composed of a different sediment facies or have a small-scale rougher surface, or both, than the lower backscatter deep seafloor. However, this interpretation is speculative due to the lack of samples from the region.

The MBES bathymetry shows large areas of bedforms along the base of the edifice and out onto the deep seafloor that appear to be ponded against Necker Ridge on the south (Fig. 8A). Bedforms were identified from the MBES bathymetry, and a slope map was generated from the MBES bathymetry. The slope map (Fig. 14) shows a large, 6700 km² field of sinuous crests and troughs that represents the undulated surface of bedforms. Bedforms occur in water depths of 3500–4500 m with downslope-concave arcuate crests with few if any bifurcations. Crest heights

decrease down slope (Fig. 15) from 1 m to 7 m, and all occur on gradients of less than 1.6°. The bedforms vary from asymmetrical to symmetrical with no apparent variation with water depth (Fig. 15). Another field of bedforms occurs off the southeast-facing margin of the French Frigate Shoals edifice that extends below a headwall scarp and slide block (Fig. 8A). This bedform field is 27 km long and 6 km wide with an upper region on a 4.5° slope that decreases to 2° near the toe (Fig. 15, profile A–B). The bedforms occur in water depths of 3200 m to 4200 m, and it is not possible to determine from the SBP profiles if either the large or small field overlaps another because of the lack of SBP penetration.

An unusual feature occurs on the SSE upper flank of the French Frigate Shoals edifice. A gently curved, 26-km-long, chute-like feature (labeled “chute” in Figs. 8A and 16) occurs ~1000 m below the edifice platform. The chute slopes down from 1800 m to 3800 m water depth at 1.5° to 2° gradients before it plunges 850 m

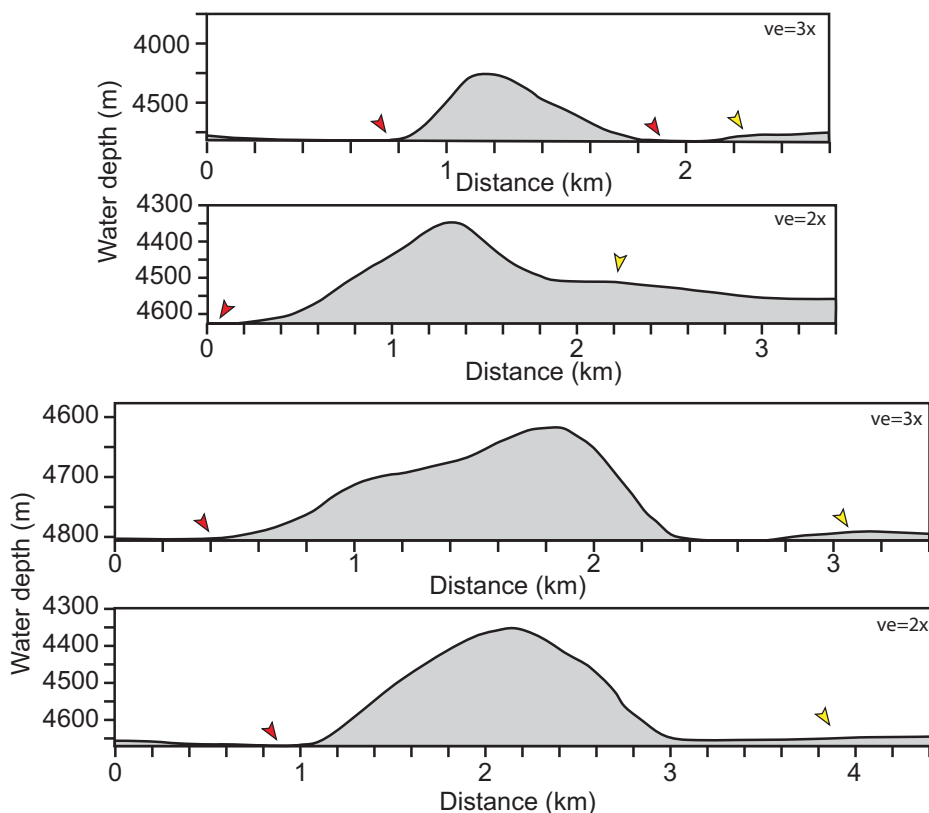


Figure 11. Down-gradient bathymetric profiles across outrunners, located by yellow arrowheads in Figure 8 (A), show banked sediment on up-gradient side (yellow arrowheads) and scour (red arrowheads) on the down-gradient side.

with a 20° gradient down to the deep seafloor at 4480 m water depth. The chute begins on the flank of the edifice at ~1800 m water depth, not at the edge of the edifice summit platform at ~200 m water depth, and it is not related to any prominent headwall scarp. Interior walls that stand 400–500 m high bound either side of the chute and confine the path of the chute for the first 24 km before a steep descent to the deep seafloor. The chute is 10 km wide throughout its length between the confining walls. Several downslope converging channels occur on the floor of the chute with high backscatter values of

–33 dB to –27 dB as compared to values of –39 to –37 dB for the inter-channel areas (Figs. 8B and 16). Channels at the head of the chute have as much as 20 m of relief on a 24-km-wide terrace with a 4° slope. The channels increase in relief to more than 80 m at the abrupt change of downslope gradient to the 20° drop-off (Fig. 17), although on slopes less than 5° the channel relief is below the resolution of the MBES bathymetry. The floor of the chute is tilted ~1° toward the eastern wall, and the channels follow this tilt to strike southeast across the chute floor until they approach the eastern wall. The channels follow

the base of the eastern wall throughout the rest of their path to the deep seafloor. A profile along the center of the chute shows three abrupt descents (Fig. 17), the largest of which descends 1000 m to the deep seafloor. The chute is positioned between areas of debris flows and outrunner blocks and has directed sediment on top of a large field of creep (Fig. 8A).

A 180-m-deep plunge pool occurs on the deep seafloor at the base of the chute (Figs. 16 and 17). The southern margin of the plunge pool is surrounded by a semicircular, 80–100-m-high rim. The backscatter of the plunge pool is –34 dB to –32 dB as compared to the –27 dB to –22 dB backscatter of the rim. Six kilometers beyond the rim, a ~2 km halo of high backscatter that varies from –31 dB to –23 dB merges to the south with more typical –40 dB backscatter of the deep seafloor.

Southern Archipelagic Apron of the Necker Island Edifice

Necker Island is a small island on a much larger 1600 km² bank at ~30 m water depth that rises from a ~3300 km² platform in water depths of 300–700 m. The upper flank of the edifice has gradients of 10° to 20°, and the lower flank has smoothly decreasing gradients from 10° to ~3°. The upper edge of the southwestern-facing flank of the edifice has four headwall scarps (Fig. 18). The largest headwall scarp is 22 km wide and located at the western upper edge of the edifice upslope from the northern termination of Necker Ridge. The landslide from this headwall scarp fed most of the debris to the French Frigate Shoals edifice side of Necker Ridge, although some debris was transported to the Necker Island edifice side. To the south-southeast, debris from the next headwall scarp, which is 23 km wide, was directed only to the Necker Island edifice side of Necker Ridge. Two additional headwall scarps occur on the southeastern upper edge of the edifice; one is 16 km wide and the other is 7.5 km wide. Another headwall scarp occurs that has incised the edge of a terrace on the mid-slope of the edifice. A 3- to 10-km-wide terrace spans 44 km on the mid-flank with water depths that vary from ~2800 m on the WNW to ~3500 m on the ESE side. Similar to what is seen on the base of the headwall scarps of the French Frigate Shoals edifice, the base of the headwall scarps of Necker Island edifice have high backscatter gullies, and some extend for more than 40 km below the headwall scarp. Some gullies show a dendric pattern whereas others cross one another and eventually converge to only a few before they drop below the resolution of the MBES. Backscatter values of the gullies are –25 dB to –21 dB as compared

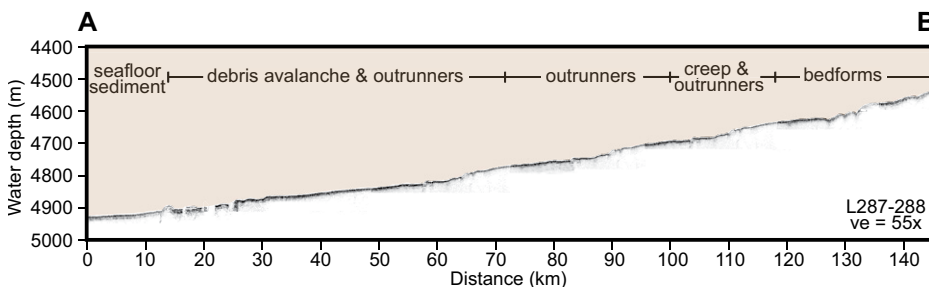


Figure 12. Sub-bottom profile L287–288 shows the seismic signatures across the French Frigate Shoals archipelagic apron. Location of profile in Figure 8B.

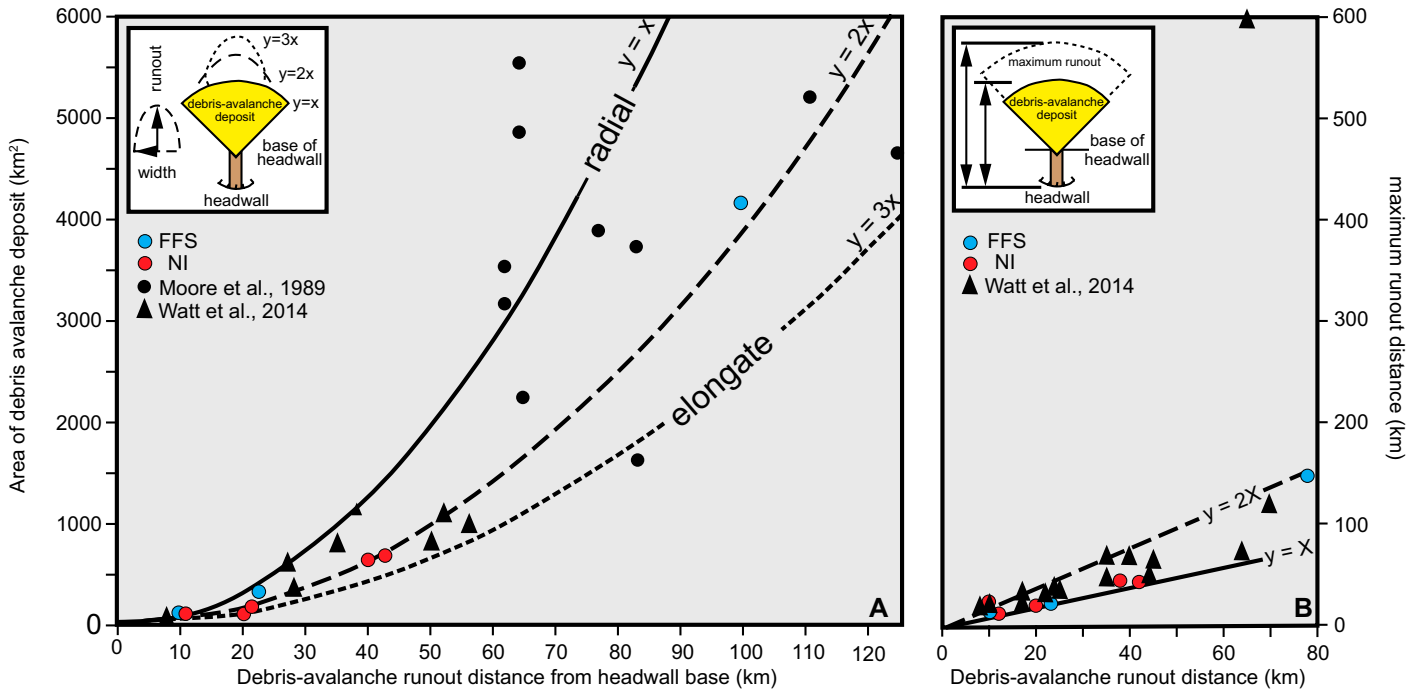


Figure 13. (A) Plot of debris avalanche areas vs. runout distance is overlain with curves of surface aspect ratio of deposits that reflects the amount of lateral spreading. **(B)** Plot of runout length of debris avalanches vs. maximum runout of total landslide deposits (modified from Watt et al., 2014). FFSE—French Frigate Shoals edifice data; NIE—Necker Island edifice data. The Moore et al. (1989) data points are from the debris avalanches off the Hawaiian Islands, and the Watt et al. (2014) data points are from various areas in the Atlantic and Caribbean.

to the -32 dB of the intervening areas. The gullies occur on upper slopes of $\sim 3^\circ$ as well as on lower slopes of less than 0.2° .

Five slides occur downslope of the headwall scarps that range in area from 20 km^2 to 175 km^2 and have thicknesses of 50 m to 400 m. Four of the five slides have estimated volumes that range from less than 0.5 km^3 to 3.5 km^3 , whereas the

fifth slide has an estimated volume of 23.3 km^3 (Fig. 10A). Estimated volumes were calculated using Equations 1 and 2. All of the slides have rough surfaces and MBES backscatter values of -30 dB to -21.5 dB as compared to the -38.5 dB to -33.5 dB backscatter immediately downslope and the -37 dB to -36 dB backscatter of the deep seafloor. The four smaller slides

all moved less than 10 km down the flank of the edifice, whereas the large slide traveled 7 km downslope. Similar to the slides on the French Frigate Shoals edifice archipelagic aprons, the estimated volumes of the Necker Island edifice slides show no correlation with seafloor gradient or distance from the base of the edifice (Figs. 10A–10B).

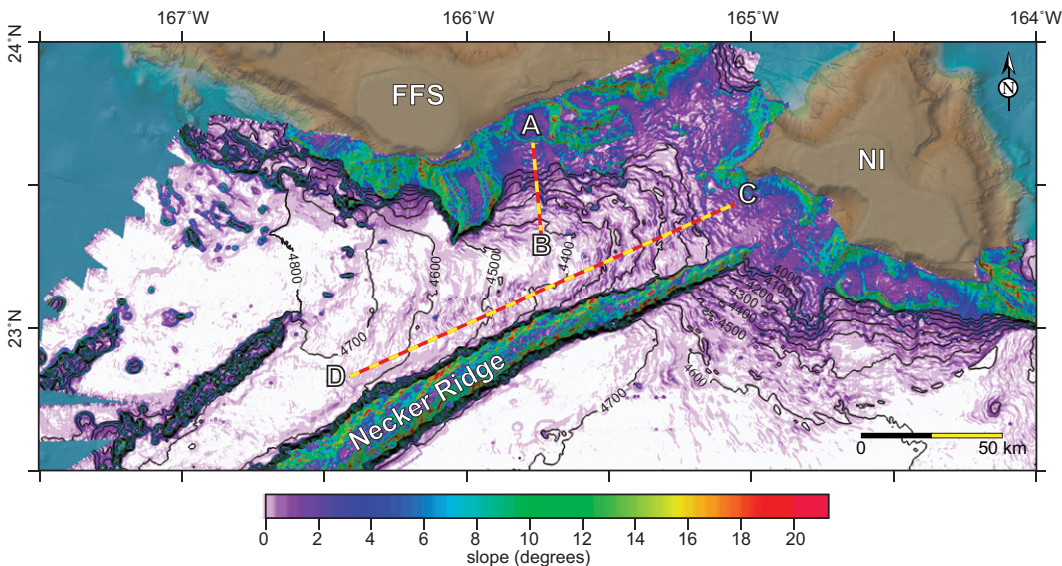


Figure 14. Slope map of multibeam echosounder bathymetry of archipelagic aprons of French Frigate Shoals (FFS) and Necker Island (NI) edifices accentuates bedforms. Iso-bath interval is 100 m. Profiles A–B and C–D are shown in Figure 15.

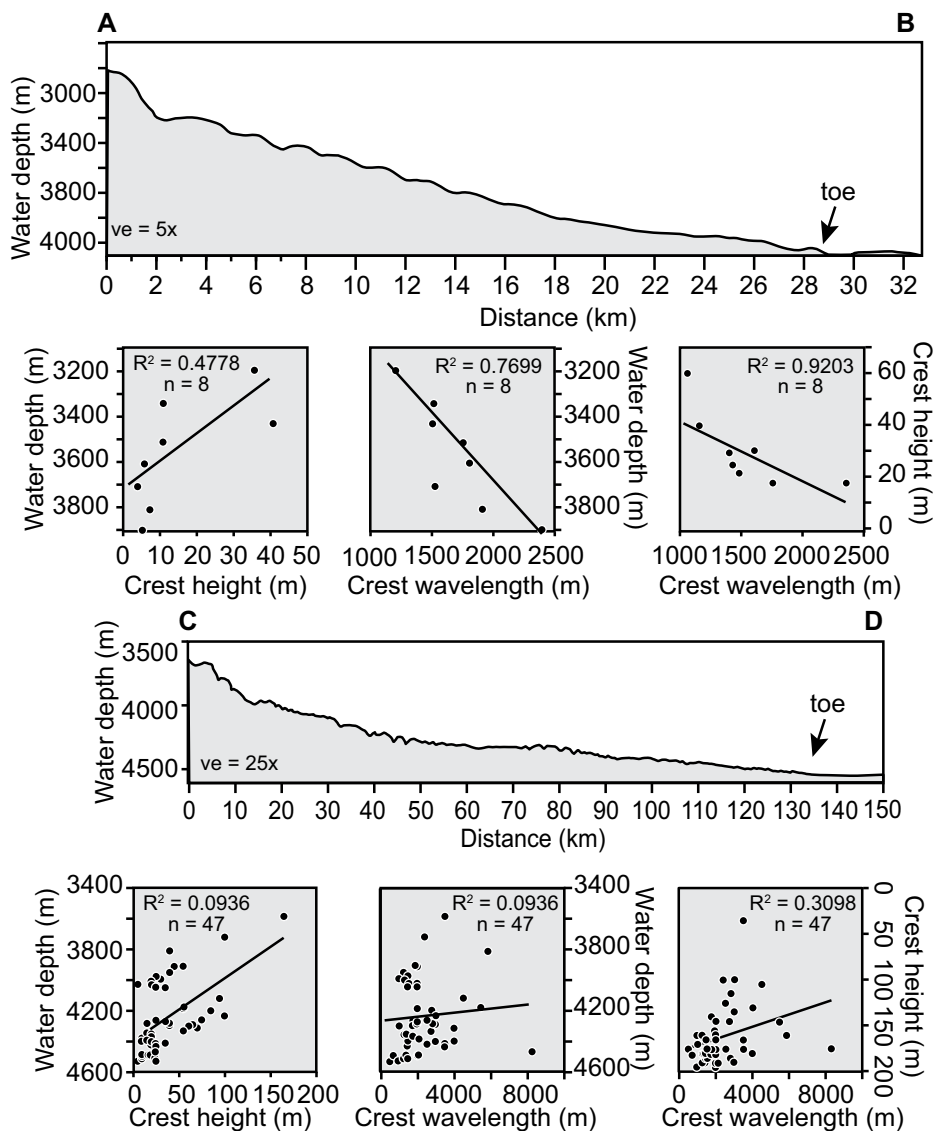


Figure 15. Bathymetric profiles A–B and C–D off the French Frigate Shoals edifice are shown with their locations. Plots below each profile show bedform crest heights and wavelengths versus water depth and crest height versus wavelength for each profile.

A large field of bedforms covers an area of at least 7680 km² that blankets the lower slopes and proximal deep seafloor southeast of Necker Ridge (Fig. 18). The bedforms extend for more than 60 km on slopes less than 2°. The crests of the bedforms have amplitudes of several meters to 20 m with wavelengths of less than 1–2 km. Shallow areas of bedforms are buried by gullies and debris avalanches that occur below some, but not all, headwall scarps. Another large field of bedforms covers at least 1320 km², was mostly generated off the Necker Island edifice and was deposited on the NW side of Necker Ridge (Figs. 18A–18B), and it extends more than 100 km onto the deep seafloor.

The bedforms and gullies are buried in places by five debris avalanches (labeled *a* through *e* in Fig. 18B). The debris avalanches range in area from 80 km² to 650 km² and occur on the upper flank of Necker Island and out on the deep seafloor. The largest debris avalanche (*a*) covers an area of 650 km² and extends at least 42 km out onto the deep seafloor. Debris avalanche (*a*) has a very elongate aspect. The next smaller debris avalanche (*b*) covers an area of 580 km² with an elongate aspect and extends 30 km downslope. The three smaller debris avalanches cover areas of 130 km² (*c*), 100 km² (*d*), and 80 (*e*) km². All are elongate in aspect and each extends less than 15 km downslope. According to Watt et al. (2014), the more radial surface aspect is the

product of a cohesionless flow with large clasts as a dominant component whereas the more elongate surface aspect is the result of a flow with a more cohesive sediment.

The surfaces of the two largest debris avalanches have mottled backscatter textures (Figs. 18C–18D) with background values of –36 dB and isolated areas with values of –21 dB as compared to values of –25.5 dB to –19.5 dB in the gully sections on either side of the debris avalanches. The low backscatter values suggest the debris avalanches are blanketed with more recent sediments. The heads of the two largest debris avalanches (*a* and *b* in Fig. 18B) occur on gradients of ~2° that abruptly flatten out to less than 0.2° as they extend 25–30 km out onto the deep seafloor. The largest debris avalanche (*a* in Figs. 10B and 19) extends 31.5 km out to the deep seafloor with a consistent width of 13.4 km throughout its length. The feature stands 350–400 m high and covers an area of 600 km². The next largest debris avalanche (*b* in Fig. 18B) is 22.5 km long, 9 km wide, stands 85 m high, and covers an area of 480 km².

Three fields of outrunners and five solitary outrunners occur downslope, where the gradient is less than 1° (Fig. 18A). Three solitary outrunners occur on the lateral edges of debris avalanche *b* in water depths deeper than 4650 m and are the farthest from the base of the edifice. The eastern field has 11 single or amalgamated outrunners and the middle field has 4 outrunners, all of which reside between the 4500 m and 4600 m isobath. Two isolated outrunners occur in 4700 m water depth on a 0.02° slope 15 km seaward from a subtle change in slope. All of the outrunners have equidimensional plan shapes (Fig. 10C) and range in estimated volume mostly less than 0.02 km³, but the three solitary outrunners are much larger with estimated volumes of 0.4 km³ and 0.7 km³.

DISCUSSION

The presence of archipelagic aprons on the lower flanks of the French Frigate Shoals and Necker Island edifices is not surprising because archipelagic aprons are common features on the flanks of islands, seamounts, and guyots. However, the presence of these archipelagic aprons brings up several obvious questions. (1) Were the bedforms that occur on the archipelagic aprons caused by slow downslope creep, or were they produced by energetic turbidity currents? (2) When did the landslide events on the archipelagic aprons occur? (3) What were the forcing mechanisms that caused them? (4) What formed the large

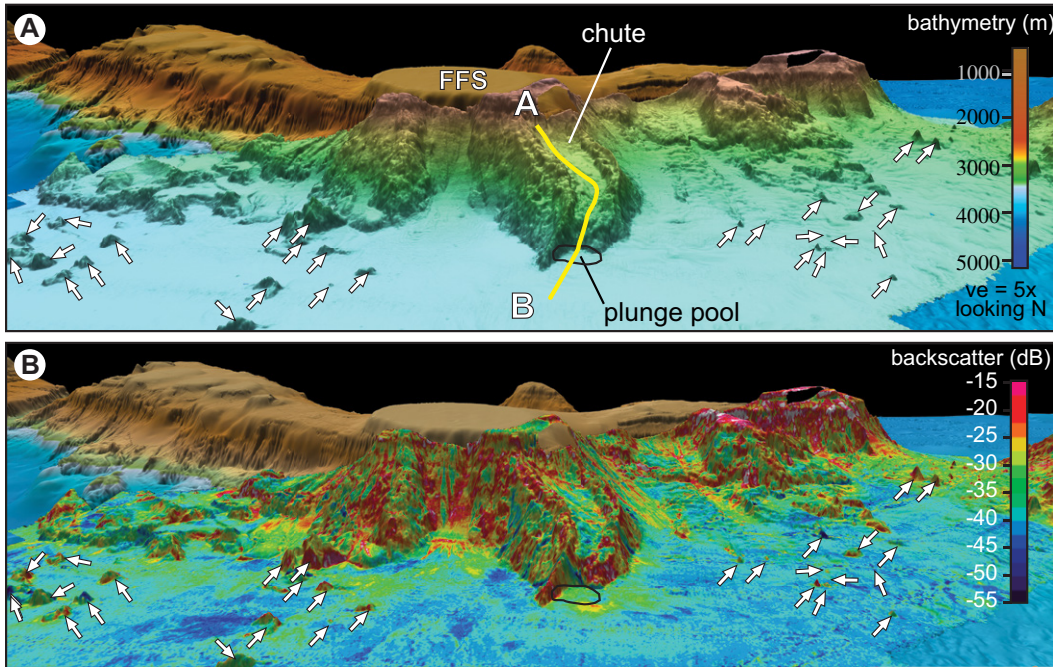


Figure 16. (A) Perspective view of multibeam echosounder bathymetry. Yellow profile A–B is the axial profile shown in Figure 17. (B) Acoustic backscatter of chute on the southern flank of French Frigate Shoals (FFS) edifice. White arrows point to outrunners. A plunge pool at the base of the chute-shaped feature is outlined in black.

chute on the south-facing flank of the French Frigate Shoals edifice?

Are the Bedforms the Result of Turbidity Currents or Sediment Creep?

Throughout the descriptions and discussions above, bedforms are described and interpreted to be evidence of slow-moving sediment creep. However, many recent studies of archipelagic aprons have described bedforms as the result of energetic turbidity currents (e.g., Wynn and Stow, 2002; Pope et al., 2018; Quartau et al., 2018; Santos et al., 2019; Casalbore et al., 2020). Individual French Frigate Shoals edifice and Necker Island edifice bedform crest heights, crest wavelengths, and water depths were measured, and plots are shown in Figures 15 and 20. Wynn and Stow (2002), Pope et al. (2018), Santos et al. (2019), and Casalbore et al. (2020), and references therein discuss criteria to distinguish between bedforms caused by turbidity currents and sediment creep. Table 1 contrasts the differences in morphology and setting discussed in these studies to distinguish bedforms formed by energetic turbidity currents from those formed by

slow, gravity-induced sediment deformation that is generally described as creep. The bedforms described from the French Frigate Shoals and Necker Island edifices more resemble features that were created by slow downslope creep due to (1) their proximal area on slopes of $\sim 2^\circ$, (2) their relatively modest runout distances, (3) the lack of confinement at the margins, (4) the lack of channels, and (5) the lack of a fluvial source that is often cited in the above references as evidence of a source for turbidity currents. The orientation of the bedform crests perpendicular to the downslope gradient precludes geostrophic currents as the process that formed the bedforms. Consequently, the bedforms are interpreted to be the result of slow downslope creep under the influence of gravity from the relatively steep upper gradients.

When Did the Landslides Occur?

The archipelagic aprons off the southern flanks of the French Frigate Shoals and Necker Island edifices are complex and mostly depositional features. MBES bathymetry and acoustic backscatter show that some of these facies bury

other facies; some are confined to the upper flanks of the edifices whereas others extend onto the deep seafloor beyond the archipelagic aprons. For example, a creep field on the southeast-facing flank of the French Frigate Shoals edifice is the main facies of the archipelagic apron (Fig. 8) and is partially covered by slides, gullies, debris avalanches, and outrunners. This suggests the creep field may be older than the overlying facies, because there is no evidence that any of the overlying deposits have been further displaced within this creep field. Another example is the large field of creep off the southern flank of the Necker Island edifice (Fig. 18). There, the large creep field has a few scattered slides, gullies, and a field of outrunners that rest on it. However, in these examples, are the various facies all part of the same landslide event or do they represent multiple events? Watt et al. (2014) argue that most submarine landslides are multiple events rather than a single event. The SBP records collected for this study rarely show penetration beneath the highly reflective surface layer (e.g., Figs. 12 and 21). Unfortunately, the only publicly available descriptions of cores are from water depths deeper than 4600 m (Fig. 6). However, one observation is especially interesting. As mentioned earlier, sediment ponding on the uphill sides and scour on the downhill sides of many outrunners suggests that some of the debris avalanches that surround outrunners may not have resulted from a single event but either represent a series of reoccurring events that occurred during a prolonged landslide event or a series of events that post-date the initial landslide.

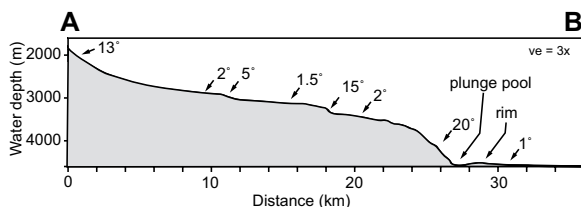


Figure 17. Axial profile of multibeam echosounder bathymetry down the center of the chute feature on flank of the French Frigate Shoals edifice is shown. Location of profile A–B is shown in Figure 16.

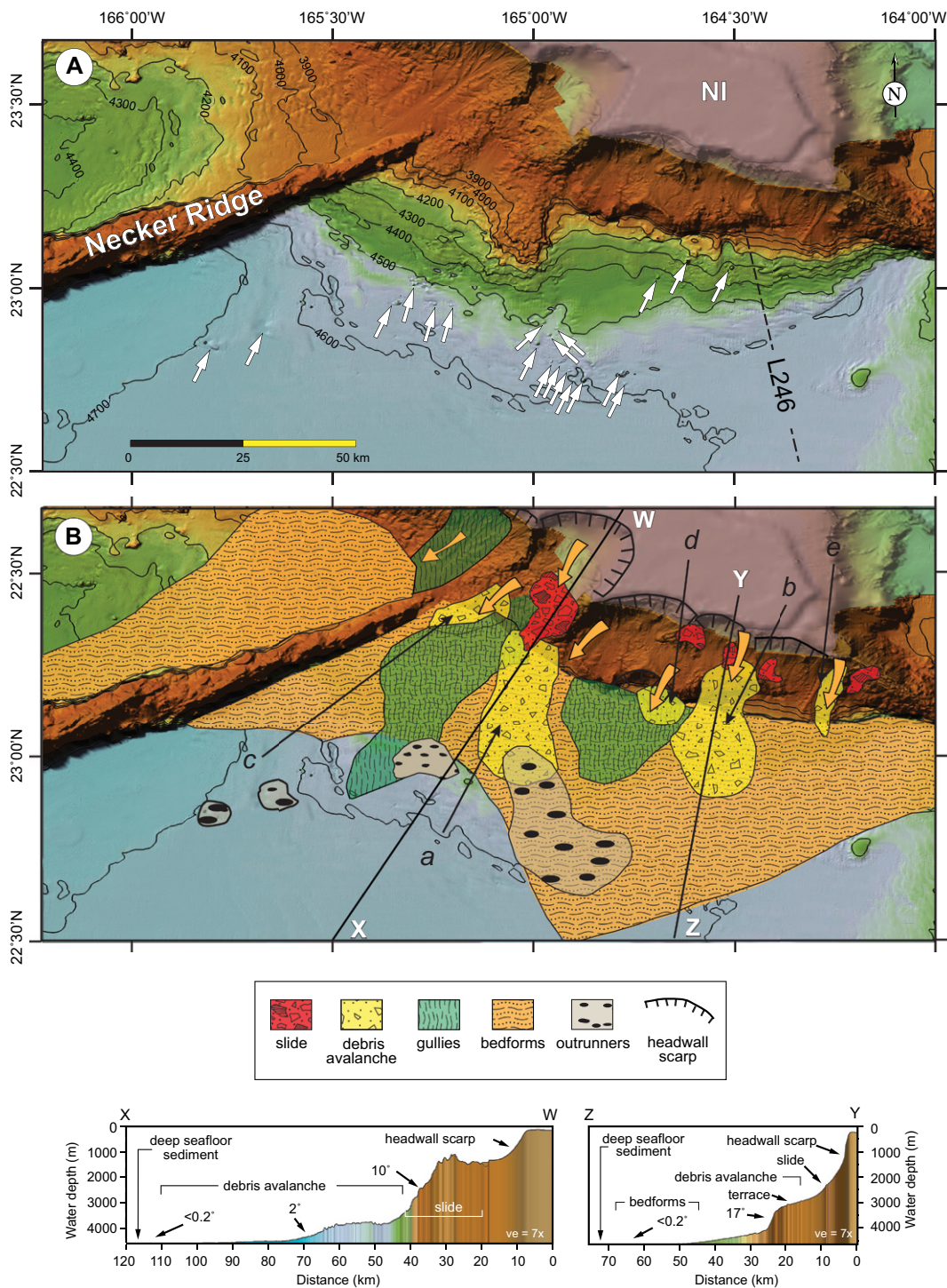


Figure 18. (A) Map view of multibeam echosounder bathymetry of Necker Island edifice (NI) archipelagic apron. Isobaths are in meters. Dashed black lines are track lines of sub-bottom profiler line L246 (see Fig. 21). White arrows in (C) point to outrunners. (B) Same area as (A) with interpretations. White arrows point to outrunners. Locations of profiles W–X and Y–Z shown line in (B). Italic letters *a–d* point to debris avalanches (see text for discussion). Parts (C) and (D) are multibeam echosounder acoustic backscatter of the same area as in (A) and (B). White arrows in (C) point to outrunners and (D) are color-coded outlines of the components of the archipelagic apron. See Figure 7 for bathymetry and backscatter color scales.

The absence of any sediment cores from the archipelagic aprons makes estimates of the ages of the landslides problematic. However, the available SBP data can suggest a relative age for some of the most recent components of the archipelagic aprons. At an average speed of ~ 50 km/m.y. (Garcia et al., 2006), the French Frigate Shoals and Necker Island edifices took ~ 22 m.y. to drift to their current

locations 1100 km from the Hawaiian hotspot. Presently, approximately the southern half of the Northwest Hawaiian Ridge between the French Frigate Shoals edifice and the island of Hawai'i has a subaerial component, whereas the northern half is submerged. Using these observations as a rough submergence history, the French Frigate Shoals and Necker volcanoes probably subsided beneath sea level

~ 6 m.y. ago. Once submerged a few hundred meters, which took perhaps another million years, a pelagic drape should have begun to accumulate. SBP profiles, with a resolution of 1 m in water depths deeper than 1000 m of the archipelagic apron due south of the Necker Island edifice, show no indication of any pelagic drape (Fig. 21). Only one SBP profile (Fig. 20B) shows any pelagic drape that blan-

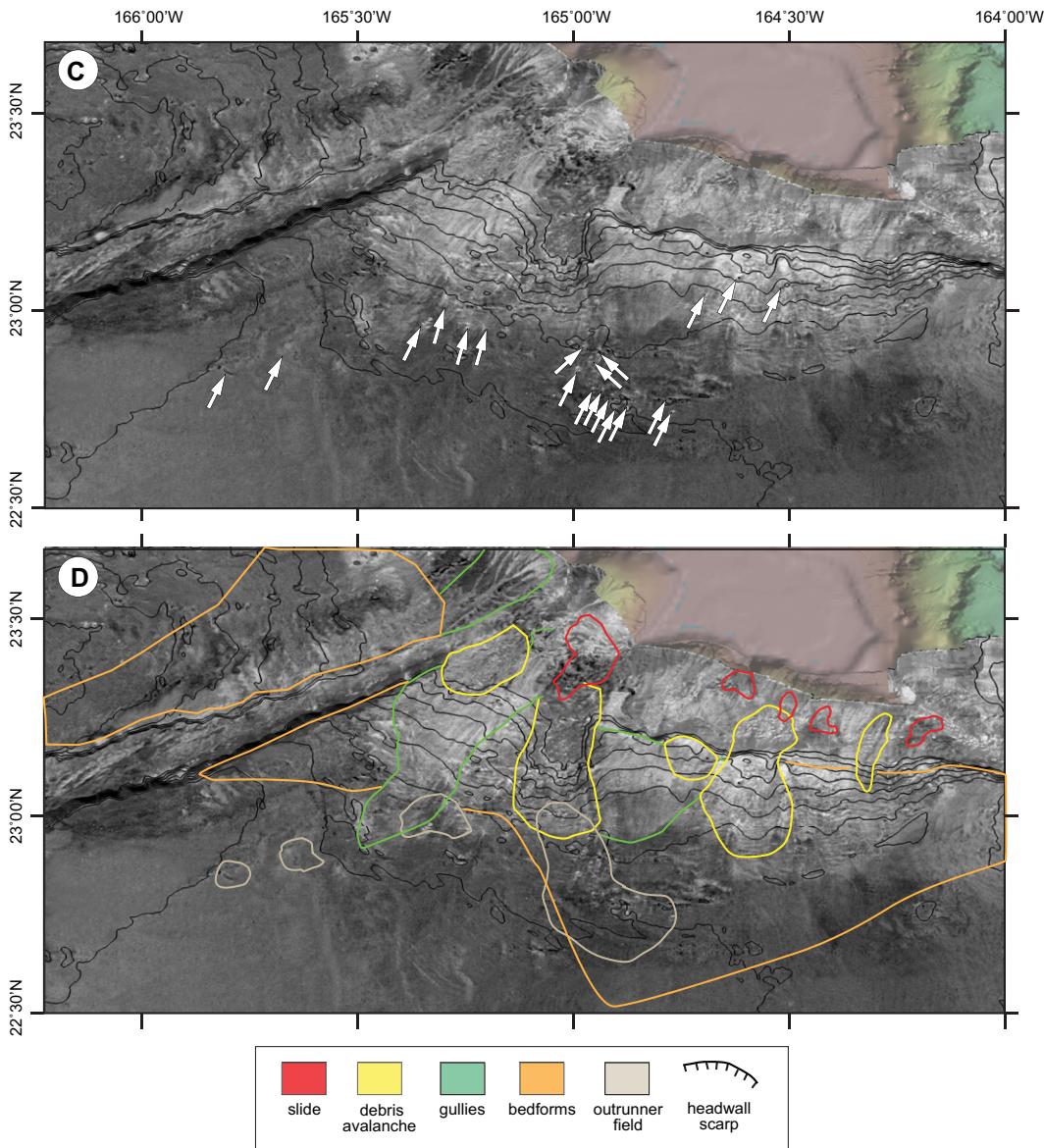


Figure 18. (Continued)

kets the seafloor. That SBP profile crosses the large area of creep sourced from the Necker Island edifice and was deposited immediately north of Necker Ridge. The pelagic drape thins from ~50 m thick at 3900 m water depth to undetectable at 4450 m water depth. The carbonate compensation depth (CCD) in this area is ~4600 m (Peterson, 1966; Berger, 1967); thus, seafloor above this depth is within the lysocline and should have accumulated pelagic drape. None of the SBP profiles show any pelagic drape at depths below the CCD depth. Pelagic carbonate sedimentation rates above the CCD in this region range from 5.8 m/m.y. from 1.7 Ma to 1 Ma and 1–0.7 m/m.y. from 1 Ma to 0.7 Ma (Moore et al., 1994). At these sedimentation rates, together with the above assumptions, a 50-m-thick section of pelagic

drape would take ca. 9 Ma to accumulate. These observations suggest that the creep field off the southwest flank of the Necker Island edifice and immediately north of Nicker Ridge is not recent in age and was probably last active in the late Tertiary. The debris avalanches and outrunners that rest on the creep field may be either contemporary or are at least certainly younger than the creep field. None of the SBP profiles across the archipelagic apron south of the Necker Island edifice (e.g., Fig. 21) and above the CCD show any pelagic drape, and thus the last Necker Island edifice landslides must be relatively recent, perhaps less than 1 Ma old, using the sedimentation rates above, a maximum pelagic sediment thickness of 1 m, and the resolution of the sub-bottom profiler at these water depths.

Potential Forcing Mechanism: Episodic or Single Events?

Keating and McGuire (2000, 2004) provide comprehensive reviews of the factors that contributed to failure of submarine volcanoes while the subaerial volcanoes were active as well as long after they became dormant and submerged. The factors they identify include: (1) variations in the degree of cementation of reefs when the edifices were close to sea level, (2) dikes intruded early in the volcanic history of the edifice, (3) seismicity both during and after volcanism, and (4) composition of the igneous rocks; and all involve gravity as the primary driving force.

The partial collapse of individual Hawaiian shield volcanoes after they became dormant is well documented (e.g., see Moore et al., 1989;

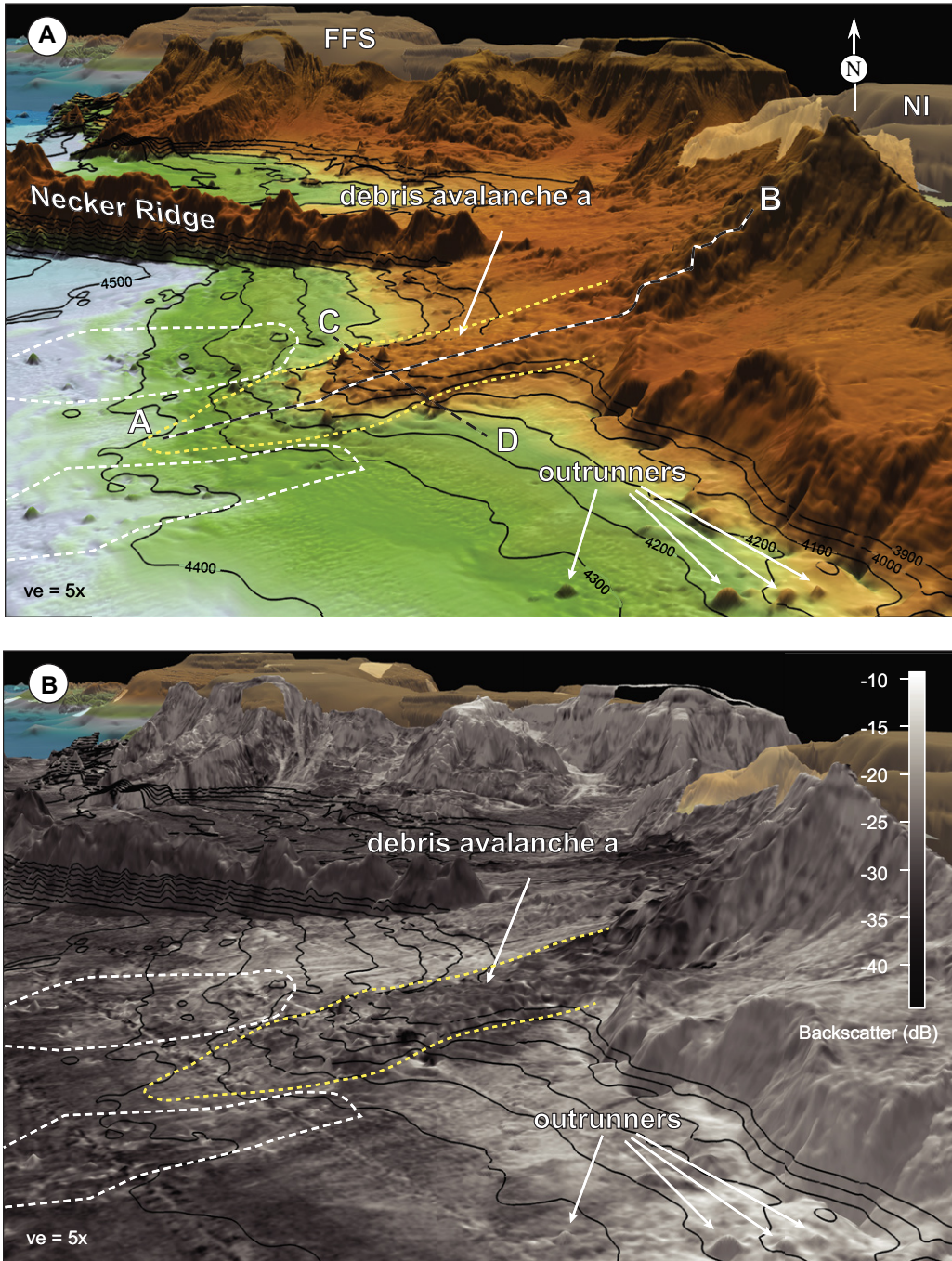
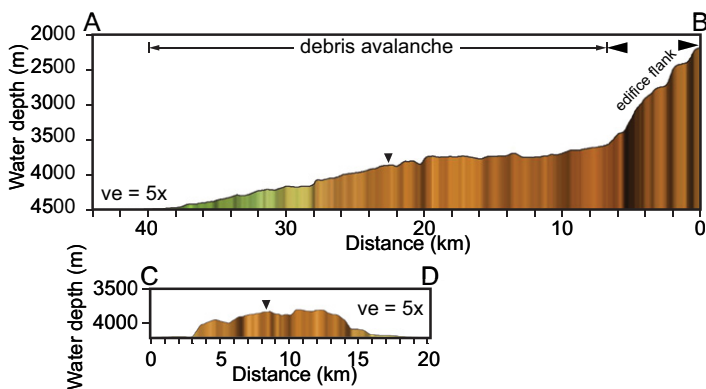


Figure 19. (A) Perspective view of multibeam echosounder bathymetry looking NNE of southern flank of Necker Island edifice (NI). (B) Acoustic backscatter image of (A). Debris avalanche A is outlined by dashed yellow line. Black and white dashed line is Profile A-B, which trends up the debris avalanche and onto the edifice flank, and black and white dashed line C-D is the profile that trends across the debris avalanche. The black arrowhead on the profiles points to the area where the profiles cross. Selected isobaths are in meters. Dashed white line is the outline of the eastern and central outrunner fields. See Figure 7 for bathymetry color scale. FFS—French Frigate Shoals.



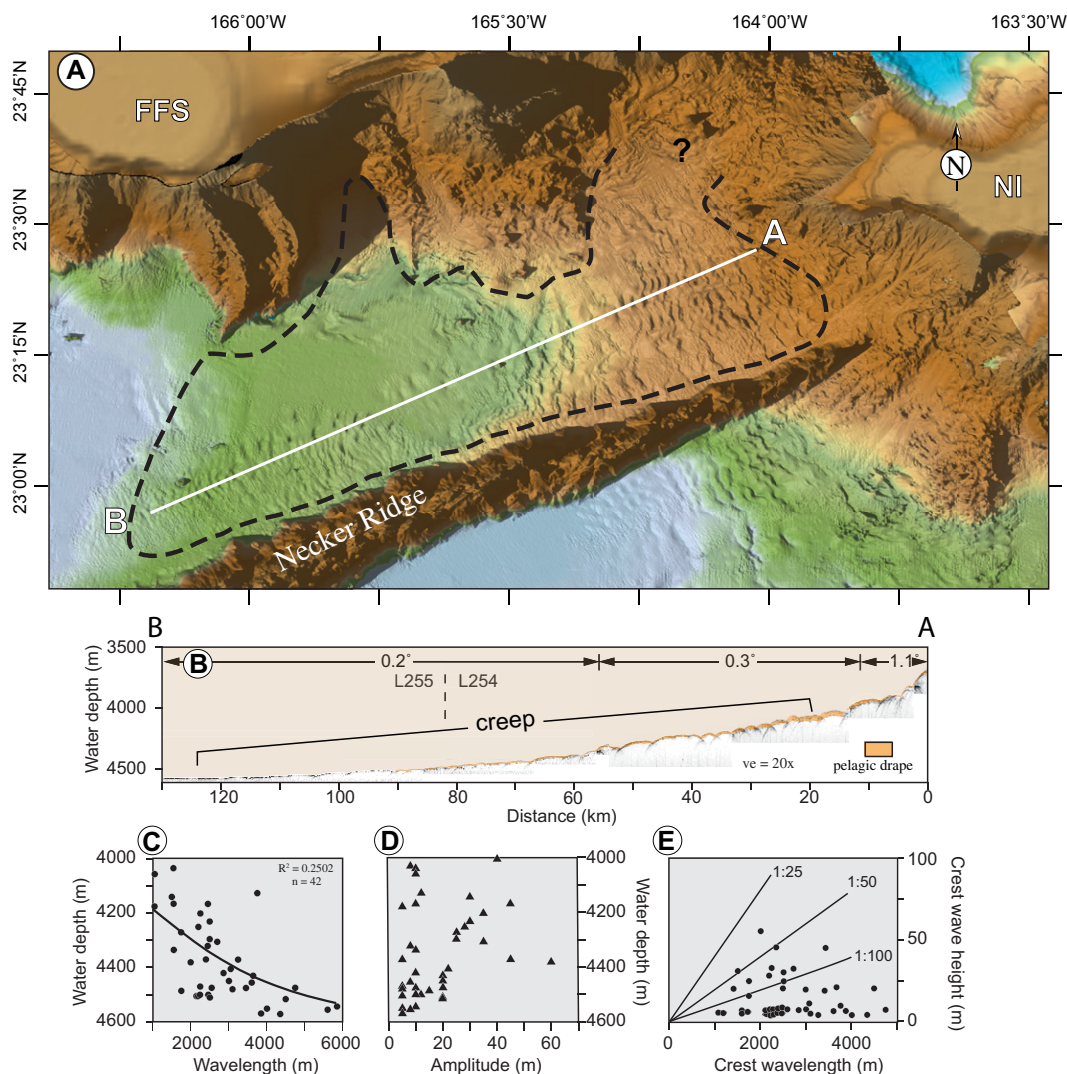


Figure 20. Map view of MBES bathymetry of large field of bedforms shed off the southeastern flank of Necker Island edifice (NI) and southern flank of French Frigate Shoals (FFS) and deposited on the NW side of Necker Ridge. Selected isobaths in meters. Dashed black line outlines field of bedforms. Solid white line is location of profile A-B. See Figure 7A for bathymetry color scale. (B) SBP line L254-255 that shows bedforms and pelagic drape (orange) that blankets the bedforms (see text for discussion). (C), (D) and (E) are plots of bedform crest heights and crest wavelengths parameters. Black lines in (E) are constant ratios of crest height to crest wavelength.

Keating and McGuire, 2000, 2004). Mass wasting generated debris avalanches and large outrunners (called slide blocks by Moore et al., 1989) after the cessation of the constructive phase of volcanism (Keating and McGuire, 2000, 2004). The prominent headwall scarps on both the French Frigate Shoals and Necker Island edifices are direct evidence of the collapse of the upper flanks and rims of the edifices. The large outrunners are undoubtedly blocks of the volcanic edifices that were eroded off the upper flanks and transported to the deep seafloor. French Frigate Shoals experienced a 5.2 Mw earthquake in 1988 with an epicenter less than 100 km from the study area (<https://www.globalcmt.org>). Consequently, seismicity long after the two edifices migrated away from the hotspot is a prime candidate for the initiation of failures on the flanks and rims of the two edifices. The presently active hotspot beneath Hawaii and Loihi is ~1100 km from French Frigate Shoals and Necker Islands. French Frigate Shoals and Necker Island are dat-

ed at 12.5–10.5 Ma, the time when the two edifices were over the Hawaiian hotspot (O'Connor, et al., 2013). Consequently, if the outrunners and distal parts of the debris avalanches occurred a few million years ago, they should be at least partially buried by at least 5 m of sediment (us-

ing abyssal clay accumulation rates of 1 m/m.y.). However, the outrunners and distal parts of the debris avalanches below the CCD do not appear to be even partially buried by abyssal clays. In addition, the headwall scarps and gullies are sharply defined in the MBES bathymetry and

TABLE 1. CHARACTERISTICS OF BEDFORMS FORMED BY TURBIDITY CURRENTS VS. CREEP

Turbidity currents	Creep
Crest wavelengths up to 10 km ^{1,2}	Crest wavelengths up to 10 km ² Crest wavelengths of 150–4500 m ⁴
Crest heights up to 10–100 m ^{1,2}	Crest heights up to 100 m ² Crest heights up to 5–200 m ³ Symmetrical, flat-topped crests ²
Symmetrical to asymmetrical crests ³ Broad crests and narrow trough ² Random scatter of bedform dimensions ² Downslope decrease in crest dimensions ^{1,2} No significant thickness ² Usually on slopes 0.1° to 0.7° ² High sedimentation rates ² Oriented perpendicular to flow direction ²	Arcuate crests ² Random scatter in bedform dimensions ² Absence of significant sediment input ¹ Most common on 2° to 5° slopes ^{2,4}
Confined and unconfined margins ^{2,3,4} Related to an upslope headscarp ² Asymmetry varies with slope ^{3,4} Presence of channels ^{2,4,5}	Oriented normal to maximum gradient ¹ No crest bifurcation ¹ Unconfined open slope ^{2,3,4} Consistent asymmetry ^{1,2} Lack of channels

Notes: ¹Lee and Chough (2001), ²Wynn and Stow (2002), ³Pope et al. (2018), ⁴Santos et al. (2019), ⁵Casalbore et al. (2020).

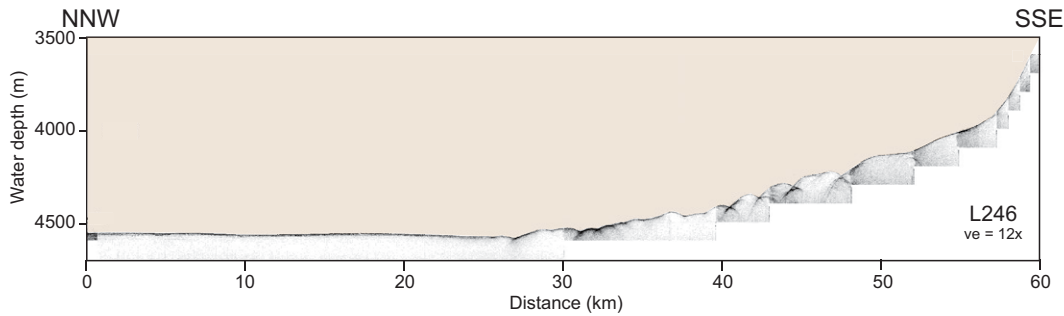


Figure 21. Sub-bottom profiler record south of the Necker Island edifice that shows the lack of sediment drape. Location of profile is shown in Figure 18A.

backscatter, which suggests the failures are relatively recent and must have occurred sometime long after volcanism ceased on the two edifices. Another possibility is that the landslides could have been a consequence of subsidence as the edifices migrated away from the mantle plume, followed by uplift, as the area was transported over the Hawaiian flexural moat. Renewed subsidence should have then occurred as the edifices subsided on the back side of the fore-arc bulge created by the flexural moat. All of the vertical tectonics could have occurred as the Pacific Plate migrated to the northwest away from the active island-building volcanism (Clague and Dalrymple, 1989; Wessel, 1993; Thordarson and Garcia, 2018). The fore-arc bulge is 200–300 km away from the active Hawai'i Island and surrounds it, so that tectonism at the French Frigate Shoals and Necker Island edifices might have uplifted and subsided the edifices sometime between ca. 3 m.y. ago and ca. 2 m.y. ago using the faster rate of 100 km/m.y. as the rate of Pacific Plate motion (O'Connor et al., 2013) as the edifices traversed the present Hawaiian flexural moat. The Hawaiian Deep at the location of the two edifices has not yet been completely filled by landslide deposits; it is ~100 m deeper than the seafloor to the southwest.

Downslope-trending gullies immediately below the headwall scarps, shown best in acoustic backscatter images (Fig. 9), appear similar to linear striations identified by Gee et al. (2005) in similar settings. Bathymetric profiles across the gullies have 2–5 m of downcutting on an otherwise low-backscatter surface. Gullies represent sediment transport that appears to have continued after the initial failures because the gullies were not buried by pelagic sedimentation.

Bedforms interpreted as creep (see above) are by far the facies that cover the largest areas of the archipelagic aprons. Creep occurs all along the southern bases of the French Frigate Shoals and Necker Island edifices (Figs. 8, 14, and 18). Creep can be generated by gradual gravitational sliding and slumping of unconsolidated sediment down a slope of lower gradients than would normally generate slides and slumps (e.g., Lee and Chough, 2001; Wynn and Stow,

2002), although many bedforms on archipelagic aprons are attributed to energetic turbidity currents (e.g., Wynn and Stow, 2002; Pope et al., 2018; Pope et al., 2018; Quartau et al., 2018; Casalbore et al., 2020). Creep is found on slopes of less than 1° all along the archipelagic aprons of the French Frigate Shoals and Necker Island edifices. The creep area off the French Frigate Shoals and Necker Island edifices that is confined to the northwest side of Necker Ridge is unusual compared to the other fields of creep in the immediate area. This area has the only bedforms with surfaces draped by acoustically transparent sediment (discussed above). The acoustically transparent nature of the drape, as well as the fact that it is a drape and not only infilling of the troughs, suggests that the drape is more than likely pelagic and not formed from volcanoclastic sediment. Additionally, the water depth where the sediment drape thins to unresolved on SBP profiles occurs at ~4450 m, which is close to the CCD in this region (Peterson, 1966; Berger, 1967). The drape is evidence that this particular creep field may be old. The other fields of creep do not have an overlying transparent drape.

The plan-view aspect ratios of the two debris avalanches provide some suggestions about their composition (Masson et al., 2002; Masson, 2006; Watt et al., 2014). Figures 8, 10C, and 18 show that the debris avalanches off both the French Frigate Shoals and Necker Island edifices have elongate aspects that suggest they were all cohesive flows and relatively mobile. The debris avalanche off the French Frigate Shoals edifice at the base of the chute (Fig. 8A) that is mostly covered by the large creep field is more radial in aspect, which suggests a low cohesive flow and less mobility.

The French Frigate Shoals Chute

One of the interesting geomorphic features mapped in this study is not part of an archipelagic apron but deserves at the least some speculation about its origin. This feature is the chute structure that extends 26 km beyond the

southern flank of the French Frigate Shoals edifice (Figs. 7, 8, and 16). The chute occurs ~600 m down the upper flank of the edifice and strikes perpendicular to the edifice flank. The feature has many characteristics of a chute; it is rimmed by high walls on each side, and it has a relatively flat floor on a gentle gradient that abruptly ends with an 800 m 20° descent to the adjacent deep seafloor. The chute clearly has a volcanic origin. Could the chute have formed due to a major event of rejuvenated volcanism on the flank of the French Frigate Shoals edifice? This type of volcanism has been observed along several hotspot volcanoes hundreds of kilometers beyond the active hotspot (see discussion by Garcia et al., 2010). Rejuvenated volcanism on the Hawaiian Ridge typically has occurred between 0.25 m.y. and 2.5 m.y. after cessation of growth at the main shield volcanoes (Bianco et al., 2005). If rejuvenated volcanism did occur at the French Frigate Shoals edifice, then could the volcanism have produced enough seismicity to trigger the landslides observed on the two edifices?

CONCLUSIONS

This study describes the surface geomorphometries of archipelagic aprons off the southern flanks of the French Frigate Shoals and Necker Island edifices in the central Northwest Hawaiian Ridge. The data sets used in this study include multibeam bathymetry and acoustic backscatter and sub-bottom profiles. The lack of seismic reflection profiles and sediment coring restricts interpretations to the surface geomorphometries of the area.

The archipelagic aprons are composed of a sequence of landslide features that include (1) headwall scarps on the upper flanks of the two edifices, (2) downslope-directed gullies on the upper slide surfaces, (3) intact slides on the upper and mid flanks, (4) debris avalanches that spread out downslope from the mid and lower flanks, (5) fields of sediment creep that blanket large areas on the lower flanks out onto the deep seafloor, and (6) outrunner blocks that are scattered on the lower flanks and deep seafloor

that have traveled as much as 85 km from the base of the edifice.

The major submarine landslides and archipelagic aprons off the French Frigate Shoals and Necker Island edifices differ in occurrence from the landslides and archipelagic aprons off the principal Hawaiian Islands. The landslides off the Hawaiian Islands occurred by oversteepening and loading during the late stages of volcanism of the islands. The initiation of the landslides on the south flanks of the French Frigate Shoals and Necker Island edifices may have resulted from vertical tectonics due to the uplift and relaxation of a peripheral bulge or isolated earthquakes long after the edifices passed well beyond the Hawaiian hotspot. The lack of pelagic drape in water depths above the CCD shown on available SBP profiles suggests that the latest landslides on the archipelagic apron off the French Frigate Shoals edifice are younger, perhaps Quaternary in age, than the latest landslides off the Necker Island edifice.

An unusual chute-like feature occurs on the southeastern side of the French Frigate Shoals edifice that suggests rejuvenated volcanism may have occurred thousands to millions of years after volcanism ceased once the edifice migrated away from the Hawaiian hotspot. Seismic activity from this volcanism is another potential process that could have generated the landslides off the two edifices.

ACKNOWLEDGMENTS

The MBES data were acquired for the U.S. Extended Continental Shelf Program. We are grateful to the technicians and crews of the NOAA Ship *Okeanos Explorer* and RV *Kilo Moana* for their dedication to our mapping of the area. Comments and constructive suggestions regarding earlier versions of this manuscript were provided by Sebastian Watt and Larry Mayer. Neil Mitchell and Rui Quartau provided comprehensive and very constructive critiques and suggestions regarding a later version of the manuscript; their assistance is greatly appreciated. However, the authors take full responsibility for the final interpretations. This work was funded by NOAA Grants NA05NOS4001153, NA15NOS4000200, and NA10NOS4000073. All data used in this paper are publicly available at the NOAA National Centers for Environmental Information (<https://maps.ngdc.noaa.gov/viewers/bathymetry/>; accessed January 2020).

REFERENCES CITED

- Allen, S.R., Hayward, B.W., and Mathews, E., 2007, A facies model for a submarine volcanoclastic apron: The Miocene Manukau Subgroup New Zealand: *Geological Society of America Bulletin*, v. 119, p. 725–742, <https://doi.org/10.1130/B26066.1>.
- Armstrong, A.A., and Calder, B.R., 2017, U.S. Extended Continental Shelf cruise to map Necker Ridge and vicinity, central Pacific Ocean (cruise report): UNH-CCOM/JHC Technical Report 17-001, 66 p., <http://ccom.unh.edu/publications> (accessed January 2021).
- Berger, W.H., 1967, Foraminiferal ooze: Solution at depths: *Science*, v. 156, p. 383–385, <https://doi.org/10.1126/science.156.3773.383>.
- Bianco, T.A., Ito, G., Becker, J.M., and Garcia, M.O., 2005, Secondary Hawaiian volcanism formed by flexural arch decompression: *Geochemistry, Geophysics, Geosystems*, v. 6, 24 p., <https://doi.org/10.1029/2005GC000945>.
- Bohannon, R.G., and Gardner, J.V., 2004, Submarine landslides of San Pedro escarpment southwest of Long Beach, California: *Marine Geology*, v. 203, p. 261–268, [https://doi.org/10.1016/S0025-3227\(03\)00309-8](https://doi.org/10.1016/S0025-3227(03)00309-8).
- Casalbore, D., Romagnoli, C., Chiocci, F., and Frezza, V., 2010, Morpho-sedimentary characteristics of the volcanoclastic apron around Stromboli Volcano (Italy): *Marine Geology*, v. 269, p. 132–148, <https://doi.org/10.1016/j.margeo.2010.01.004>.
- Casalbore, D., Clare, M.A., Pope, E.L., Quartau, R., Bosman, A., Chiocci, F.L., Romagnoli, C., and Santos, R., 2020, Bedforms on the submarine flanks of insular volcanoes: New insights gained from high resolution seafloor surveys: *Sedimentology*, <https://doi.org/10.1111/sed.12725>.
- Clague, D.A., and Dalrymple, G.B., 1975, Cretaceous K-Ar ages of volcanic rocks from the Musicians seamounts and the Hawaiian ridge: *Geophysical Research Letters*, v. 2, p. 305–308, <https://doi.org/10.1029/GL002i007p00305>.
- Clague, D.A., and Dalrymple, G.B., 1989, Tectonics, geochronology, and origin of the Hawaiian-Emperor volcanic chain, in Winterer, E.L., Hussong, D.M., and Decker, R.W., eds., *The Eastern Pacific Ocean and Hawaii*: Boulder, Colorado, Geological Society of America, *The Geology of North America*, v. N, p. 187–217.
- Clare, M.A., Le Bas, T., Price, D.M., Hunt, J.E., Sear, D., Cartigny, M.J.B., Vellinga, A., Symons, W., Firth, C., and Cronin, S., 2018, Complex and cascading triggering of submarine landslides and turbidity currents at volcanic islands revealed from integration of high-resolution onshore and offshore surveys: *Frontiers of Earth Science*, v. 6, p. 223, <https://doi.org/10.3389/feart.2018.00223>.
- Counts, J.W., Jorry, S.J., Leroux, E., Miramontes, E., and Jouet, G., 2018, Sedimentation adjacent to atolls and volcano-cored carbonate platforms in the Mozambique Channel (SW Indian Ocean): *Marine Geology*, v. 404, p. 41–59, <https://doi.org/10.1016/j.margeo.2018.07.003>.
- Dalrymple, G.B., Lanphere, M.A., and Jackson, E.D., 1974, Contributions to the petrography and geochronology of volcanic rocks from the Leeward Hawaiian Islands: *Geological Society of America Bulletin*, v. 85, p. 727–738.
- Dietz, R.S., and Menard, H.W., 1953, Hawaiian Swell, Deep, and Arch, and subsidence of the Hawaiian Islands: *The Journal of Geology*, v. 61, p. 99–113, <https://doi.org/10.1086/626059>.
- Dietz, R.S., Menard, H.W., and Hamilton, E.L., 1954, Echograms of the Mid-Pacific expedition: *Deep-Sea Research*, v. 1, p. 258–273, [https://doi.org/10.1016/0146-6313\(54\)90008-8](https://doi.org/10.1016/0146-6313(54)90008-8).
- Deplus, C., Le Friant, A., Boudon, G., Komorowski, J.-C., Villemant, B., Harford, C., Ségoufin, J., and Cheminée, J.-L., 2001, Submarine evidence for large-scale debris avalanches in the Lesser Antilles Arc: *Earth and Planetary Science Letters*, v. 192, p. 145–157, [https://doi.org/10.1016/S0012-821X\(01\)00444-7](https://doi.org/10.1016/S0012-821X(01)00444-7).
- Funck, T., Dickmann, T., Rihm, R., Krastel, S., Lykke-Andersen, H., and Schmincke, H.-U., 1996, Reflection seismic investigations in the volcanoclastic apron of Gran Canaria and implications for its volcanic evolution: *Geophysical Journal International*, v. 125, p. 519–536, <https://doi.org/10.1111/j.1365-246X.1996.tb00015.x>.
- Garcia, M.O., Caplan-Auerbach, J., De Carlo, E.H., Kurz, M.D., and Becker, N., 2006, Geology, geochemistry and earthquake history of Loihi Seamount, Hawaii's youngest volcano: *Cheme de Erde Geochemistry*, v. 66, p. 81–108, <https://doi.org/10.1016/j.chemer.2005.09.002>.
- Garcia, M.O., Swinnard, L., Weis, D., Greene, A.R., Tagami, T., Sano, J., and Gandy, C.E., 2010, Petrology, geochemistry and geochronology of Kaua'i lavas over 4–5 Myr: Implications for the origin of rejuvenated volcanism and the evolution of the Hawaiian plume: *Journal of Petrology*, v. 51, p. 1507–1540, <https://doi.org/10.1093/ptrology/egq027>.
- Gardner, J.V., and Calder, B.R., 2011, U.S. Extended Continental Shelf cruise to map Necker Ridge and vicinity, central Pacific Ocean (cruise report): UNH-CCOM/JHC Technical Report 11–001, 63 p., <https://scholars.unh.edu/ccom/1252/>.
- Gardner, J.V., Calder, B.R., and Malik, M., 2013, Geomorphometry and processes that built Necker Ridge, central North Pacific Ocean: *Marine Geology*, v. 346, p. 310–325, <https://doi.org/10.1016/j.margeo.2013.09.014>.
- Gee, M.J.R., Gawthorpe, R.L., and Friedmann, J.S., 2005, Giant striations at the base of a submarine landslide: *Marine Geology*, v. 214, p. 287–294, <https://doi.org/10.1016/j.margeo.2004.09.003>.
- Geisslinger, A., Hidschleber, H.B., Schnaubelt, M., Daño-beitia, J.J., and Gallart, J., 1996, Mapping of volcanic apron and the upper crust between Gran Canaria and Tenerife (Canary Islands) with seismic reflection profiling: *Geo-Marine Letters*, v. 16, p. 57–64, <https://doi.org/10.1007/BF02202599>.
- Goldstrand, P.M., 1998, Provenance and sedimentologic variations of turbidite and slump deposits at Sites 955 and 956, in Weaver, P.P.E., Schmincke, H.-U., Firth, J.V., and Duffield, W., eds., *Proceedings of the Ocean Drilling Program, Scientific Results, Volume 157*: College Station, Texas, Ocean Drilling Program, p. 343–360.
- Hamilton, E.L., 1956, Sunken Islands of the Mid-Pacific Mountains: *Geological Society of America Memoir* 64, 97 p.
- Hess, H.H., 1946, Drowned ancient islands of the Pacific Basin: *American Journal of Science*, v. 244, p. 772–791, <https://doi.org/10.2475/ajs.244.11.772>.
- Holcomb, R.T., and Searle, R.C., 1991, Large landslides from oceanic volcanoes: *Marine Geotechnology*, v. 10, p. 19–32, <https://doi.org/10.1080/10641199109379880>.
- Hollister, C.D., Glenn, M.F., and Lonsdale, P.F., 1978, Morphology of seamounts in the western Pacific and Philippine Basin from multibeam sonar data: *Earth and Planetary Science Letters*, v. 41, p. 405–418, [https://doi.org/10.1016/0012-821X\(78\)90172-3](https://doi.org/10.1016/0012-821X(78)90172-3).
- Hungr, O., Evans, S.G., Bovis, M.J., and Hutchinson, J.N., 2001, A review of the classification of landslides of the flow type: *Environmental & Engineering Geoscience*, v. 7, p. 221–238, <https://doi.org/10.2113/gseengeosci.7.3.221>.
- Hunt, J.E., and Jarvis, I., 2020, The lifecycle of mid-ocean ridge seamounts and their prodigious flank collapses: *Earth and Planetary Science Letters*, v. 530, no. 115867, <https://doi.org/10.1016/j.epsl.2019.115867>.
- Jones, J.G., 1967, Clastic rocks of Espiritu Santo Island: New Hebrides: *Geological Society of America Bulletin*, v. 78, p. 1281–1288, [https://doi.org/10.1130/0016-7606\(1967\)78\[1281:CROESI\]2.0.CO;2](https://doi.org/10.1130/0016-7606(1967)78[1281:CROESI]2.0.CO;2).
- Keating, B.H., and McGuire, W.J., 2000, Island edifice failures and associated tsunami hazards: *Pure and Applied Geophysics*, v. 157, p. 899–955, <https://doi.org/10.1007/s00240050011>.
- Keating, B.H., and McGuire, W.J., 2004, Instability and structural failure at volcanic ocean islands and the climate change dimension: *Advances in Geophysics*, v. 47, p. 175–271, [https://doi.org/10.1016/S0065-2687\(04\)47004-6](https://doi.org/10.1016/S0065-2687(04)47004-6).
- Kuenen, Ph.H., 1950, *Marine Geology*: New York, John Wiley & Sons, Inc., 568 p.
- Laberg, J.S., and Vorren, T.O., 2000, The Traenadjupet slide, offshore Norway—morphology, evacuation and triggering mechanisms: *Marine Geology*, v. 171, p. 95–114, [https://doi.org/10.1016/S0025-3227\(00\)00112-2](https://doi.org/10.1016/S0025-3227(00)00112-2).
- Lee, S.H., and Chough, S.K., 2001, High-resolution (2–7 kHz) acoustic and geometric characters of submarine creep deposits in the South Korea Plateau, East Sea: *Sedimentology*, v. 48, p. 629–644, <https://doi.org/10.1046/j.1365-3091.2001.00383.x>.
- Lipman, P.W., Normark, W.R., Moore, J.G., Wilson, J.B., and Guttmacher, C.E., 1988, The giant submarine Alike debris slide, Mauna Loa, Hawaii: *Journal of Geophysical Research: Solid Earth*, v. 93, p. 4279–4299, <https://doi.org/10.1029/JB093iB05p04279>.
- Malik, M., Verplanck, N., Lobecker, E., Stuart, E., Sheeham, J., LeBarage, A., Hunt, J., and Colello, B., 2009, EX0909L1 Mapping field trials Leg 1 Necker Ridge: NOAA Cruise Report, 25 p., <https://repository.library.noaa.gov/view/noaa/12571> (accessed January 2021).

- Manville, V., Németh, K., and Kano, K., 2009, Source to sink: A review of three decades of progress in the understanding of volcanoclastic processes, deposits, and hazards: *Sedimentary Geology*, v. 220, p. 136–161, <https://doi.org/10.1016/j.sedgeo.2009.04.022>.
- Masson, D.G., 2006, Catastrophic collapse of the volcano island of Hierro 15 ka ago and the history of landslides in the Canary Islands: *Geology*, v. 15, p. 231–234.
- Masson, D.G., Kidd, R.B., Gardner, J.V., Huggett, Q.J., and Weaver, P.P.E., 1992, Saharan continental rise: Facies distribution and sediment slides, in Poag, C.W., and de Graciansky, P.C., eds., *Geologic Evolution of Atlantic Continental Rises*: New York, Van Nostrand Reinhold, p. 327–343, https://doi.org/10.1007/978-1-4684-6500-6_13.
- Masson, D.G., Watts, A.B., Gee, M.J.R., Urgeles, R., Mitchell, N.C., Le Bas, T.P., and Canals, M., 2002, Slope failures on the flanks of the western Canary Islands: *Earth-Science Reviews*, v. 57, p. 1–35, [https://doi.org/10.1016/S0012-8252\(01\)00069-1](https://doi.org/10.1016/S0012-8252(01)00069-1).
- McGuire, W.J., 1996, Volcano instability: A review of contemporary themes, in McGuire, W.J., Jones, A.P., and Neuberg, J., eds., *Volcano Instability on the Earth and Other Planets*: Geological Society, London, Special Publication 110, p. 1–23, <https://doi.org/10.1144/GSL.SP.1996.110.01.01>.
- McGuire, W.J., 2006, Lateral collapse and tsunamigenic potential of marine volcanoes, in Troise, C., DeNatale, G., and Kilburn, C.R.J., eds., *Mechanisms of Activity and Unrest at Large Calderas*: Geological Society, London, Special Publication 269, p. 121–140, <https://doi.org/10.1144/GSL.SP.2006.269.01.08>.
- Menard, H.W., 1956, Archipelagic aprons: *Bulletin of the American Association of Petroleum Geologists*, v. 40, p. 2195–2210.
- Menard, H.W., 1964, *Marine Geology of the Pacific*: New York, McGraw-Hill Book Co., 271 p.
- Mitchell, N.C., 2003, Susceptibility of mid-ocean ridge volcanic islands and seamounts to large-scale landsliding: *Journal of Geophysical Research: Solid Earth*, v. 108, <https://doi.org/10.1029/2002JB001997>.
- Mitchell, N.C., Masson, D.G., Watts, A.B., Gee, M.J.R., and Urgeles, R., 2002, The morphology of the submarine flanks of volcanic ocean islands: A comparative study of the Canary and Hawaiian hotspot islands: *Journal of Volcanology and Geothermal Research*, v. 115, p. 83–107, [https://doi.org/10.1016/S0377-0273\(01\)00310-9](https://doi.org/10.1016/S0377-0273(01)00310-9).
- Montanaro, C., and Beget, J., 2011, Volcano collapse along the Aleutian Ridge (western Aleutian Arc): *Natural Hazards and Earth System Sciences*, v. 11, p. 715–730, <https://doi.org/10.5194/nhess-11-715-2011>.
- Moore, J.G., and Clague, D.A., 2002, Mapping of the Nuanu and Wailau landslides in Hawaii, in Takahashi, E., Lipman, P.W., Garcia, M.O., Naka, J., and Armaki, S., eds., *Hawaiian Volcanoes: Deep Underwater Perspectives*: Washington, D.C., American Geophysical Union Monograph 128, p. 223–244.
- Moore, J.G., Clague, D.A., Holcomb, R.T., Lipman, P.W., Normark, W.R., and Torresan, M.E., 1989, Prodigious submarine landslides on the Hawaiian Ridge: *Journal of Geophysical Research: Solid Earth*, v. 94, p. 17,465–17,484, <https://doi.org/10.1029/JB094iB12p17465>.
- Moore, J.G., Normark, W.R., and Holcomb, R.T., 1994, Giant Hawaiian Landslides: Annual Review of Earth and Planetary Sciences, v. 22, p. 119–144, <https://doi.org/10.1146/annurev.ea.22.050194.001003>.
- O'Connor, J.M., Steinberger, B., Regelous, M., Koppers, A.A.P., Hasse, K.M., Stoffers, P., Jokat, W., and Garbe-Schönberg, D., 2013, Constraints on past plate and mantle motion from new ages for the Hawaiian-Emperor Seamount Chain: *Geochemistry, Geophysics, Geosystems*, v. 14, <https://doi.org/10.1002/ggge.20267>.
- Peterson, M.N.A., 1966, Calcite: Rates of dissolution in a vertical profile in the central Pacific: *Science*, v. 154, p. 1542–1544, <https://doi.org/10.1126/science.154.3756.1542>.
- Pope, E.L., Jutzeler, M., Cartigny, M.J.B., Shreeve, J., Talling, P.J., Wright, I.C., and Wyszczanski, R.J., 2018, Origin of spectacular fields of submarine sediment waves around volcanic islands: *Earth and Planetary Science Letters*, v. 493, p. 12–24, <https://doi.org/10.1016/j.epsl.2018.04.020>.
- Posamentier, H.W., and Kolla, V., 2003, Seismic geomorphology and stratigraphy of depositional elements in deep-water settings: *Journal of Sedimentary Research*, v. 73, p. 367–388, <https://doi.org/10.1306/111302730367>.
- Quartau, R., Ramalho, R.S., Maderia, J., Santos, R., Rodrigues, A., Roque, C., Carrara, G., and Brum da Silveira, A., 2018, Gravitational, erosional and depositional processes on volcanic ocean islands: Insights from submarine morphology of Madeira Archipelago: *Earth and Planetary Science Letters*, v. 482, p. 288–299, <https://doi.org/10.1016/j.epsl.2017.11.003>.
- Ramalho, R.S., Winckler, G., Maderia, J., Helffirich, G.R., Hipelto, A., Quartau, R., Adena, K., and Schaefer, J.M., 2015, Hazard potential of volcanic flank collapses raised by new megatsunami evidence: *Science Advances*, v. 1, no. 1500456, <https://doi.org/10.1126/sciadv.1500456>.
- Rooney, J.J., Wessel, P., Hoeke, R., Weiss, J., Baker, J., Parrish, F., Fletcher, C.H., Chojnacki, J., Garcia, M., Brainard, R., and Vroom, R., 2008, Geology and geomorphology of coral reefs in the northeastern Hawaiian Islands, in Riegl, B.M., and Dodge, R.E., eds., *Coral Reefs of the USA: Dordrecht, Springer Science & Business Media, B.V.*, p. 519–572, https://doi.org/10.1007/978-1-4020-6847-8_13.
- Ryan, W.B.F., Carbotte, S.M., Coplan, J.O., O'Hara, S., Melkonian, A., Arko, R., Weissel, R., Ferrini, V., Goodwillie, A., Nitsche, F., Bonczkowski, J., and Zemsky, R., 2009, Global multi-resolution topography synthesis: *Geochemistry, Geophysics, Geosystems*, v. 10, <https://doi.org/10.1029/2008GC002332>.
- Saint-Ange, F., Bachèlery, P., Babonneau, N., Michon, L., and Stephan, J.J., 2013, Volcanoclastic sedimentation on the submarine slopes of a basaltic hotspot volcano: Piton de la Fournaise volcano (La Réunion Island, Indian Ocean): *Marine Geology*, v. 337, p. 35–52, <https://doi.org/10.1016/j.margeo.2013.01.004>.
- Saito, K., and Ozima, M., 1977, ⁴⁰Ar/³⁹Ar geochronological studies of submarine rocks from the western Pacific area: *Earth and Planetary Science Letters*, v. 33, p. 353–367, [https://doi.org/10.1016/0012-821X\(77\)90087-5](https://doi.org/10.1016/0012-821X(77)90087-5).
- Santos, R., Quartau, R., Brum da Silveira, A., Ramalho, R., and Rodrigues, A., 2019, Gravitational, erosional, sedimentary and volcanic processes on the submarine environment of Selvagens Islands (Madeira Archipelago, Portugal): *Marine Geology*, v. 415, no. 105945, <https://doi.org/10.1016/j.margeo.2019.05.004>.
- Schmincke, H.-U., Weaver, P.P.E., and Firth, J.V., et al., 1995, Background, objectives, and principal results of drilling the clastic apron of Gran Canaria (VICAP), in *Proceedings of the Ocean Drilling Program, Initial Report, Volume 157*: College Station, Texas, Ocean Drilling Program, p. 11–25.
- Shepard, F.P., 1963, *Submarine Geology*, 2nd Edition: New York, Harper & Row, Publishers, 557 p.
- Smoot, N.C., 1982, Guyots in the mid-Emperor chain mapped with multibeam sonar: *Marine Geology*, v. 47, p. 153–163, [https://doi.org/10.1016/0025-3227\(82\)90024-X](https://doi.org/10.1016/0025-3227(82)90024-X).
- Smoot, N.C., 1983a, Guyots of the Dutton Ridge at the Bonin/Mariana trench juncture as shown by multi-beam surveys: *The Journal of Geology*, v. 91, p. 211–220, <https://doi.org/10.1086/628757>.
- Smoot, N.C., 1983b, Multi-beam surveys of the Michelson Ridge guyots: Subduction or obduction: *Tectonophysics*, v. 99, p. 363–380, [https://doi.org/10.1016/0040-1951\(83\)90113-0](https://doi.org/10.1016/0040-1951(83)90113-0).
- Smoot, N.C., 1985, Observations of Gulf of Alaska seamount chains by multi-beam sonar: *Tectonophysics*, v. 115, p. 235–246, [https://doi.org/10.1016/0040-1951\(85\)90140-4](https://doi.org/10.1016/0040-1951(85)90140-4).
- Taylor, P.T., Stanley, D.J., Simkin, T., and Jahn, W., 1975, Gilliss Seamount: Detailed bathymetry and modification by bottom currents: *Marine Geology*, v. 19, p. 139–157, [https://doi.org/10.1016/0025-3227\(75\)90066-3](https://doi.org/10.1016/0025-3227(75)90066-3).
- Taylor, P.T., Wood, C.A., and O'Hearn, T.J., 1980, Morphological investigation of submarine volcanism: Henderson seamount: *Geology*, v. 8, p. 390–395, [https://doi.org/10.1130/0091-7613\(1980\)8<390:MIOSVH>2.0.CO;2](https://doi.org/10.1130/0091-7613(1980)8<390:MIOSVH>2.0.CO;2).
- Thordarson, T., and Garcia, M.O., 2018, Variance of the flexure model predictions with rejuvenated volcanism at Kilauea Point, Kauai, Hawaii: *Frontiers of Earth Science*, v. 4, <https://doi.org/10.3389/feart.2018.00121>.
- Vogt, P.R., and Smoot, N.C., 1984, The Geisha Guyots: Multibeam bathymetry and morphometric interpretation: *Journal of Geophysical Research: Solid Earth*, v. 89, p. 11,085–11,107, <https://doi.org/10.1029/JB089iB13p11085>.
- Watson, J.J., Whittaker, J.M., Lucieer, V., Coffin, M.F., and Lamarche, G., 2017, Erosional and depositional processes on the submarine flanks of Ontong Java and Nukumanu atolls, western equatorial Pacific Ocean: *Marine Geology*, v. 392, p. 122–139, <https://doi.org/10.1016/j.margeo.2017.08.006>.
- Watt, S.F.L., 2015, New insights into landslide processes around volcanic islands from remotely operated vehicle (ROV) operations offshore Montserrat: *Geochemistry, Geophysics, Geosystems*, v. 16, p. 2240–2261, <https://doi.org/10.1002/2015GC005781>.
- Watt, S.F.L., Talling, P.J., Vardy, M.E., Masson, D.G., Henstock, T.J., Hühnerback, V., Minshull, T.A., Urlaub, M., Lebas, E., Le Friant, A., Berndt, C., Crutchley, G.J., and Karstens, J., 2012a, Widespread and progressive seafloor-sediment failure following volcanic debris avalanche emplacement: Landslide dynamics and timing offshore Montserrat: *Marine Geology*, v. 323–325, p. 69–94, <https://doi.org/10.1016/j.margeo.2012.08.002>.
- Watt, S.F.L., Talling, P.J., Vardy, M.E., Heller, V., Hühnerback, V., Urlaub, M., Sarkar, S., Masson, D.G., Henstock, T.J., Minshull, T.A., Paulatto, M., Le Friant, A., Lebas, E., Berndt, C., Crutchley, G.J., Karstens, J., Stinton, A.J.K., and Maeno, F., 2012b, Combinations of volcanic-flank and seafloor-sediment failure offshore Montserrat, and their implications for tsunami generation: *Earth and Planetary Science Letters*, v. 319–320, p. 228–240, <https://doi.org/10.1016/j.epsl.2011.11.032>.
- Watt, S.F.L., Talling, P.J., and Hunt, J.E., 2014, New insights into the emplacement dynamics of volcanic island landslides: *Oceanography*, v. 27, p. 46–57, <https://doi.org/10.5670/oceanog.2014.39>.
- Watts, A.B., 1978, An analysis of isostasy in the world's oceans, I. Hawaiian-Emperor seamount chain: *Journal of Geophysical Research: Solid Earth*, v. 83, p. 5989–6004, <https://doi.org/10.1029/JB083iB12p05989>.
- Wessel, P., 1993, A reexamination of the flexural deformation beneath the Hawaiian Islands: *Journal of Geophysical Research: Solid Earth*, v. 98, p. 12,177–12,190, <https://doi.org/10.1029/93JB00523>.
- Wolfe, C.J., McNutt, M.K., and Detrick, R.S., 1994, The Marquesas archipelagic apron: Seismic stratigraphy and implications for volcano growth, mass wasting, and crustal underplating: *Journal of Geophysical Research: Solid Earth*, v. 99, p. 13,591–13,608, <https://doi.org/10.1029/94JB00686>.
- Wynn, R.B., and Stow, D.A.V., 2002, Classification and characterization of deep-water sediment waves: *Marine Geology*, v. 192, p. 7–22, [https://doi.org/10.1016/S0025-3227\(02\)00547-9](https://doi.org/10.1016/S0025-3227(02)00547-9).

SCIENCE EDITOR: ROB STRACHAN

ASSOCIATE EDITOR: EMMANUEL GABET

MANUSCRIPT RECEIVED 29 AUGUST 2020

REVISED MANUSCRIPT RECEIVED 18 DECEMBER 2020

MANUSCRIPT ACCEPTED 13 JANUARY 2021

Printed in the USA